IMAGES IV: strong evolution of the oxygen abundance in gaseous phases of intermediate mass galaxies from z 0.8

M. Rodrigues, F. Hammer, H. Flores, M. Puech, Y. C. Liang, I. Fuentes-Carrera, N. Nesvadba, M. Lehnert, Y. Yang, P. Amram, et al.

A&A 492, 371–388 (2008)
DOI: 10.1051/0004-6361:200810435

Astronomy & Astrophysics

IMAGES IV⋆: strong evolution of the oxygen abundance in gaseous phases of intermediate mass galaxies from $z \sim 0.8$

M. Rodrigues[1,2], F. Hammer[1], H. Flores[1], M. Puech[3,1], Y. C. Liang[4], I. Fuentes-Carrera[1], N. Nesvadba[1], M. Lehnert[1], Y. Yang[1], P. Amram[5], C. Balkowski[1], C. Cesarsky[1], H. Dannerbauer[6], R. Delgado[1,7], B. Guiderdoni[8], A. Kembhavi[9], B. Neichel[1], G. Östlin[10], L. Pozzetti[11], C. D. Ravikumar[12], A. Rawat[1,9], S. di Serego Alighieri[13], D. Vergani[14,11], J. Vernet[3], and H. Wozniak[8]

[1] GEPI , Observatoire de Paris, CNRS, University Paris Diderot, 5 place Jules Janssen, 92195 Meudon, France
e-mail: myriam.rodrigues@obspm.fr
[2] CENTRA, Instituto Superior Tecnico, Av. Rovisco Pais 1049-001 Lisboa, Portugal
[3] ESO, Karl-Schwarzschild-Strasse 2, 85748 Garching bei München, Germany
[4] National Astronomical Observatories, Chinese Academy of Sciences, 20A Datun Road, Chaoyang District, Beijing 100012, PR China
[5] Laboratoire d'Astrophysique de Marseille, Observatoire Astronomique de Marseille-Provence, 2 place Le Verrier, 13248 Marseille, France
[6] MPIA, Königstuhl 17, 69117 Heidelberg, Germany
[7] IFARHU-SENACYT, Technological University of Panama, 0819-07289 Panama, Rep. of Panama
[8] Centre de Recherche Astronomique de Lyon, 9 Avenue Charles André, 69561 Saint-Genis-Laval Cedex, France
[9] Inter-University Centre for Astronomy and Astrophysics, Post Bag 4, Ganeshkhind, Pune 411007, India
[10] Stockholm Observatory, AlbaNova University Center, Stockholms Center for Physics, Astronomy and Biotechnology, Roslagstullsbacken 21, 10691 Stockholm, Sweden
[11] INAF - Osservatorio Astronomico di Bologna, via Ranzani 1, 40127 Bologna, Italy
[12] Department of Physics, University of Calicut, Kerala 673635, India
[13] INAF, Osservatorio Astrofisico di Arcetri, Largo Enrico Fermi 5, 50125 Florence, Italy
[14] IASF-INAF - via Bassini 15, 20133 Milano, Italy

Received 20 June 2008 / Accepted 21 September 2008

ABSTRACT

Context. Intermediate mass galaxies ($>10^{10}$ $M_\odot$) at $z \sim 0.6$ are the likeliest progenitors of the present-day, numerous population of spirals. There is growing evidence that they have evolved rapidly in the last 6 to 8 Gyr, and likely already have formed a significant fraction of their stellar mass, often showing perturbed morphologies and kinematics.
Aims. We have gathered a representative sample of 88 such galaxies and have provided robust estimates of their gas phase metallicity.
Methods. We used moderate spectral resolution spectroscopy at VLT/FORS2 with an unprecedentedly high S/N allowing us to remove biases coming from interstellar absorption lines and extinction, to establish robust values of R_{23} = ([OII]λ3727 + [OIII]$\lambda\lambda$4959, 5007)/Hβ.
Results. We definitively confirm that the predominant population of $z \sim 0.6$ starbursts and luminous IR galaxies (LIRGs) are on average two times less metal rich than the local galaxies at a given stellar mass. We do find that the metal abundance of the gaseous phase of galaxies evolves linearly with time, from $z = 1$ to $z = 0$ and after comparing with other studies, from $z = 3$ to $z = 0$. Combining our results with the reported evolution of the Tully Fisher relation, we find that such an evolution requires that ∼30% of the stellar mass of local galaxies have been formed through an external supply of gas, thus excluding the closed box model. Distant starbursts & LIRGs have properties (metal abundance, star formation efficiency & morphologies) similar to those of local LIRGs. Their underlying physics is likely dominated by gas infall, probably through merging or interactions.
Conclusions. Our study further supports the rapid evolution of $z \sim 0.4$–1 galaxies. Gas exchange between galaxies is likely the main cause of this evolution.

Key words. galaxies: evolution – galaxies: ISM – galaxies: spiral – galaxies: starburst – infrared: galaxies

1. Introduction

There is a growing consensus that most of the decline of star-formation density since $z = 1$ is related to the strong evolution in the intermediate-mass galaxy population, with $M_{\rm stel}$ from 1.5 to 15 $\times$ 10^{10} $M_\odot$ (Hammer et al. 2005; Bell et al. 2005). At intermediate redshift these galaxies are progenitors of present day spirals. This work belongs to a series of studies on intermediate-mass galaxies at $z \sim 0.6$, in the framework of the large program IMAGES (Intermediate MAss Galaxy Evolution Sequence). In Paper I (Yang et al. 2008), we present the 2D kinematics of a representative sample of 65 galaxies and put into evidence the high fraction of non-relaxed galaxies at this redshift. In Paper II (Neichel et al. 2008), we establish a morpho-kinematical classification and find a strong evolution of the fraction of well-relaxed spiral rotating disk in the last 6 Gyr. We also point out that intermediate-mass galaxies have doubled their stellar mass since $z \sim 0.6$ according to the evolution of the

⋆ Intermediate MAss Galaxy Evolution Sequence, ESO programs 174.B-0328(B), 174.B-0328(F), 174.B-0328(K), 66.A-0599(A).

Tully-Fisher relation found in Paper 3 (Puech et al. 2008). As a whole, this series of papers has shown that intermediate-mass galaxies have undergone a strong evolution of their kinematical and morphological properties since $z \sim 0.6$. These results reveal the agitated history of spiral disk galaxies over the last 6 Gyr.

The evolution of the metal content of the gas in galaxies is a useful tool to probe various galaxy evolution scenarios. In fact, the stellar mass-metallicity relation (M-Z) can help to disentangle the contribution of several processes taking place during galaxy evolution such as the star-formation history, outflow powered by supernovae or stellar winds and infall of gas by merger or secular accretion. In the local Universe the M-Z relation has been widely studied since Lequeux et al. (1979). Tremonti et al. (2004) performed a reliable estimation of oxygen abundance and stellar mass for 53 000 star-forming galaxies from the SDSS. Several studies have characterized the relation at higher redshift: $0 < z < 1$ (Kobulnicky & Kewley 2004; Liang et al. 2006; Savaglio et al. 2005; Lamareille et al. 2007), $1 \leq z \leq 2$ (Liu et al. 2008; Erb et al. 2006; Shapley et al. 2004; Maier et al. 2006) and $z \geq 3$ (Maiolino et al. 2008). A significant evolution is found as a function of redshift: $z \sim 0.7$ galaxies show on average a gaseous abundance with a factor of two less than local counterparts at a given stellar mass (Liang et al. 2006). Such a trend is also found at higher redshift. However, the metal abundance of the gas in galaxies is estimated for all these samples from strong line calibrations such as R_{23} which uses [O III], [O II] and Hβ or $N2$, which uses [N II] and Hα. Several parameters affect the measurement of line ratios: extinction and underlying Balmer absorption in the case of R_{23}, the unknown contribution of primary nitrogen production as a function of the metallicity for $N2$, and for both parameters the spectral resolution. Liang et al. (2004b) emphasized the necessity of a spectral resolution of $R > 1000$ and a $S/N > 10$ to recover robust physical quantities from spectra. There are still few studies reaching the spectral quality necessary to estimate reliable metal abundances for intermediate redshift galaxies. The data from the Keck Redshift Survey are limited by the absence of flux calibration, making it impossible to estimate the extinction. Moreover, metallicity estimated using the equivalent widths produces systematically higher metal abundances (Liang et al. 2006). Savaglio et al. (2005) observed 56 galaxies from the Gemini Deep Deep Survey with flux-calibrated spectra, but the S/N of the data were insufficient to measure extinction for individual galaxies.

The aim of this paper is to obtain a robust M-Z relation for a reasonably large sample of intermediate mass galaxies at $z \sim 0.6$. In this paper, we have followed the methodology proposed by Liang et al. (2006) consisting of a precise estimate of the extinction and underlying Balmer absorption in order to obtain reliable R_{23} abundance determinations. The high quality spectra were taken with the VLT/FORS2. The paper is organized as follows: Sect. 2 describes the observational data and discusses the completeness of the sample. In Sect. 3, we outline the methodology followed to estimate extinction, star-formation rates and metallicities, as well as determine the contribution of AGN. Results concerning the evolution of the M-Z relation and the effect of galaxy morphology are given in Sect. 4. In Sect. 5, we discuss systematic effects and the implication of our results for the closed box scenario. We summarize our conclusions in Sect. 6.

Throughout this paper we adopt a Λ-CDM cosmological model ($H_0 = 70$ km s^{-1} Mpc^{-1}, $\Omega_M = 0.3$ and $\Omega_\Lambda = 0.7$). All magnitudes used in this paper are in the AB system, unless explicitly noted otherwise. The adopted solar abundance is $12 + \log(O/H) = 8.66$ from Asplund et al. (2004).

Table 1. The number and type of objects in the redshift quality classes: secure (2) for spectra contain more than two strong feature, insecure (1) when only one features was detected but with not very reliable supporting features, and single emission line (9) when the spectra had a single emission line without any features.

Class	Galaxy	Star	QSO	Total	%
2	169	19	4	192	83
1	32	–	–	32	14
9	7	–	–	7	3
Total	208	19	4	231	–

2. IMAGES observation

2.1. VLT/FORS2 Observations

Galaxies were observed with the VLT/FORS2 in the Chandra Deep Field South (CDFS) in the context of the ESO large program "IMAGES". We randomly selected 270 galaxies in 4 fields of $6'8 \times 6'8$. Observations were performed in MXU mode, using two holographic grisms, GRIS 600RI+19 and GRIS 600z + 23, at a spectral resolution of 6.8 Å and covering a maximum wavelength range from 5120 Å to 10 700 Å. The slit masks were prepared using the GOODS catalogue (Giavalisco et al. 2004) and FORS2 pre-images. The arrangement of the slits were optimized to improve the number of objects observed. 270 slits have been placed among which 241 objects have $I_{AB} < 23.5$ mag. The minimum exposure time of each object in each grism is around 3 h.

Spectra were extracted and wavelength calibrated using the IRAF[1] package. The spectra were flux calibrated using photometric standard stars. We compared the spectrophotometry to HST/ACS photometry in V, I, Z bands and V, I, R in the EIS catalogue and found a good agreement.

2.2. Samples

From the 241 target objects with $I_{AB} < 23.5$ mag from the FORS2–IMAGES sample, we have identified 231 targets. For 10 targets we have not been able to perform an identification because of instrumental problems (target falling outside the slit or bad sky extraction). Each redshift is associated with a quality flag denoting the reliability of the identification, see description in Ravikumar et al. (2007). We have classified objects into 4 types: a galaxy, split into emission line galaxies (ELG) and absorption line galaxies (ALG); quasars and stars. Table 1 shows the number and type of objects in the different redshift quality classes. From the 270 slits of the FORS2–IMAGES, we have estimated the redshift for 240 objects, giving a success rate of ~88%. For objects with $I_{AB} < 23.5$ mag the success rate reached ~96%. In Fig. 1, we have plotted the redshift histogram for all galaxies and QSO. The distribution has a range of [0.01–3.499] and a median value of 0.667. Two main peaks are visible in the redshift distribution at $z = 0.670$, $z = 0.735$. These peaks correspond to structures in the CDFS field, already identified in Ravikumar et al. (2007).

From the $I_{AB} < 23.5$ mag objects we have selected 74 galaxies that have [O II], Hβ, [O III] emission lines, in order to evaluate their metallicities. Table 2 describes the construction of the working sample by the availability of spectral lines. From the sample of 74 galaxies, we have excluded 6 objects because of

[1] IRAF is distributed by the National Optical Astronomical Observatories, which is operated by the Association of Universities for Research in Astronomy, Inc., under cooperative agreement with the National Science Foundation.

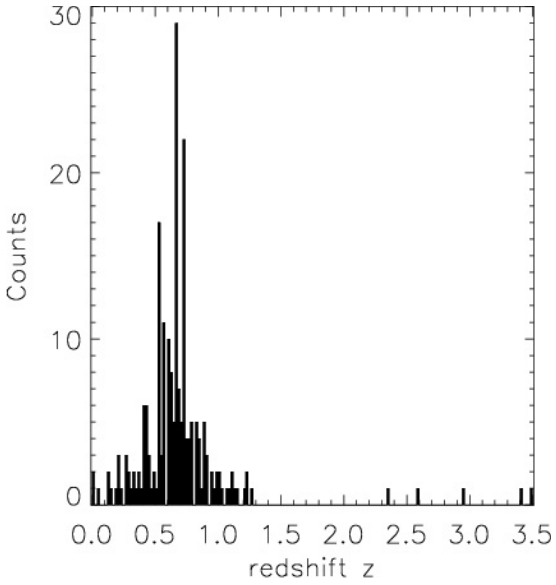

Fig. 1. Redshift distribution (bin = 0.02) of the FORS2–IMAGES sample, including the classes 2(secure), 1(insecure) and 9(single line).

bad spectrophotometry or wavelength calibration problems and 10 objects with Hβ or both [O III] lines corrupted by strong sky emission or absorption lines. Finally, our sample, hereafter sample A, is composed of 58 galaxies with a median redshift of 0.7. The S/N of the Hβ line has a mean value of 40.

The CDFS field has the advantage of being a widely studied field. The Great Observatories Origins Deep Survey (GOODS) (Giavalisco et al. 2004) provides deep multiwavelength observations. HST/ACS and EIS photometries (Arnouts et al. 2001) have been used to check the spectrophotometry and to calculate the aperture correction. The IR luminosity of galaxies has been estimated from the mid-IR catalogue of Le Floc'h et al. (2005) and using the procedure of Chary & Elbaz (2001). Observations in X-rays from the *Chandra X-Ray Observatory 1 Ms* observations (Giacconi et al. 2002) and radio detection from the Australia Telescope Compact Array 1.4 GHz (Afonso et al. 2006) have been used to identify Active Galactic Nuclei (AGN), see Sect. 3.3. The rest frame magnitude in J, K-band and the luminosity at 2800 Å have been derived by modeling galaxy SEDs using ISAAC and ACS multi-band photometry. Puech et al. (2008) have evaluated that the random uncertainty of this method is less than 0.2~mag in M_K. A catalogue of Sample A with RA, Dec, z, $I_{\rm AB}$ from the ACS, M_K, M_J, $L_{\rm IR}$ is given in Table 6.

We have completed our sample with 30 galaxies from Liang et al. (2006), referred hereafter as sample B. These $I_{\rm AB} < 22.5$ mag galaxies have been randomly selected in Canada France Redshift Survey (CFRS) 3h, Ultra Deep Survey Rosat (UDSR) and Ultra Deep Survey FIRBACK (UDSF) fields and observed with VLT/FORS2/MXU. This sample has M_K measurements and mid-IR detection obtained with ISOCAM, see Hammer et al. (2005) and Liang et al. (2004a) for a complete description.

2.3. Completeness

In this work, we have combined samples A and B and called the whole sample: sample A+B with a total of 88 galaxies. The two samples of galaxies span the same redshift range. In terms of absolute magnitude, sample B is composed of galaxies brighter than sample A. However, the combination of these two samples gives a sample representative of the intermediate mass galaxies at $z \sim 0.6$. Figure 2 shows the distribution of the K-band absolute magnitudes of sample A + B and the objects with redshift identification in the FORS2–IMAGES sample verifying $I_{\rm AB} < 23.5$ mag. We have compared, on the same plot, the luminosity distribution to the luminosity function at a redshift of 0.5 and 1 from Pozzetti et al. (2003). Kolmogorov-Smirnov tests support that sample A+B follows the LF at a 85% probability in the redshift range $z = 0.4$ and $z = 0.98$, and with $M_K < -21.5$. The corresponding stellar mass range of completeness is $\log(M_{\rm stellar}/M_\odot) > 10$. The aim of the IMAGES large program is to investigate intermediate mass galaxies with $M_{\rm stellar} > 1.5 \times 10^{10}\, M_\odot$, which represents 76% of our sample. Then, the incompleteness of the sample below $M_K = -21.5$ does not affect our conclusions.

Table 2. Number of galaxies (208 galaxies + 4 QSO) by spectral type in the IMAGES and selected sample: [O II], Hβ, [O III] and H$_\alpha$ emission lines detected (E1); [O II], Hβ, [O III] detected (E2); [O II] out of the wavelength range (E3); Hβ or/and [O III] out of range (E4); one or two emission lines detected (E5); galaxies without emission lines (Abs). The E3 galaxies correspond to low-redshift objects. In this work we have only selected the 5 galaxies with $z > 0.4$.

	E1	E2	E3	E4	E5	Abs	Total
IMAGES	4	65	20	31	49	43	212
Sample A	4	65	5	–	–	–	74

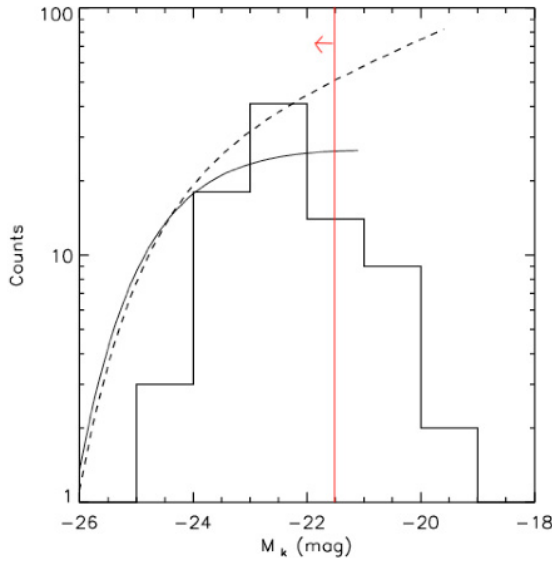

Fig. 2. Number counts (on a logarithmic scale) of selected galaxies versus AB absolute magnitude in K-band. The black histogram refers to sample A + B galaxies. The luminosity function derived from Pozzetti et al. (2003) at $z = 0.50$ is plotted with a dashed line and at $z = 1$ with solid line. The red vertical line represents the limit of 85% completeness.

3. Methodology and data analysis

The following section describes the methodology of data analysis for the sample A. The description for the sample B is given in Liang et al. (2004a) and Liang et al. (2006). The methodology used for sample A is very similar to the one used for sample B, thus the two sample are homogeneous.

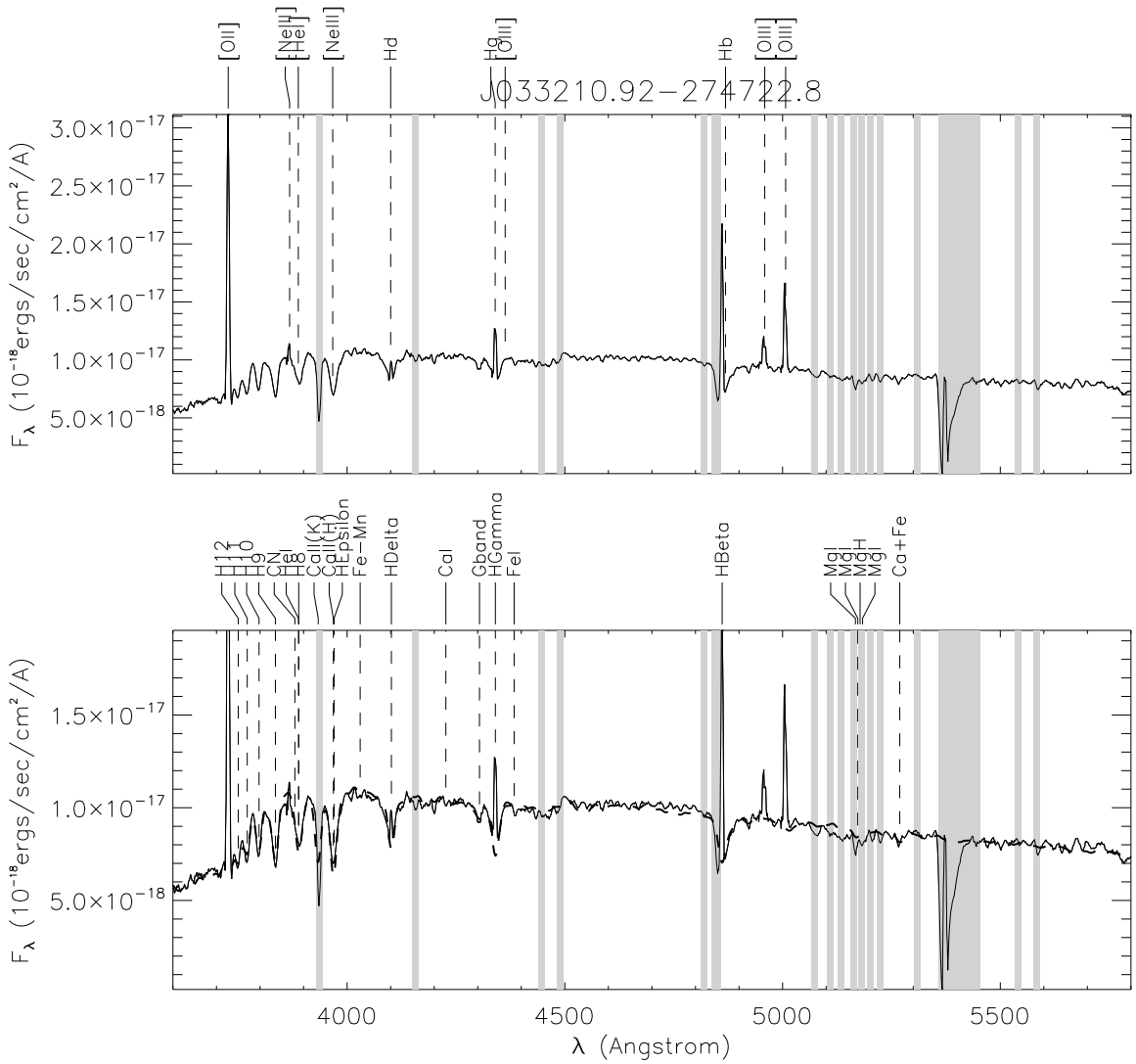

Fig. 3. Rest-frame spectrum of one of the sample A galaxies, J033210.92–274722.8. Grey boxes delimit the wavelength region where spectra may be affected by strong sky lines. *Top panel*: spectrum with the location of strong emission lines. *Bottom panel*: spectrum and synthetic spectra using Jacoby et al. (1984) templates plotted with dashed line. The position of the absorption lines are marked with dashed vertical lines.

3.1. Flux measurement

In order to derive the metal abundance in galaxies with sufficient accuracy, it is necessary to estimate the extinction and the underlying Balmer absorption. We have corrected for the Balmer emission lines from the underlying stellar population. For each galaxy, we fitted the observed spectrum, including its continuum and absorption lines, with a linear combination of stellar libraries. We have used a set of 15 stellar spectra from the Jacoby et al. (1984) stellar library, including B to M stars (e.g. B, A, F, G, K and M) with stellar metallicity. Spectra and stellar templates have been degraded to the same spectral resolution of 8 Å. The smoothing of the spectra emphasises the absorption features used in the fit. Only the continuum and absorption lines have been smoothed in the galaxy spectra. We have convolved the continuum, except at the location of emission lines, using the software developed by our group (Hammer et al. 2001). The best fit was obtained with the STARLIGHT software (Cid Fernandes et al. 2005). A Cardelli et al. (1989) reddening law has been assumed. A rest-frame spectrum of one typical galaxy of our sample, J033210.92–274722.8, is given in Fig. 3.

We have chosen to use stellar templates rather than the usually used SSP models of Bruzual & Charlot (2003), hereafter BC03. Indeed, BC03 models overestimate the absorption in the Hβ line. Asari et al. (2007); Cid Fernandes et al. (2005) have suggested that the origin of this biais is due to the STELIB library used in the BC03 models. The STELIB spectra have an excess of flux in both sides of the Hβ when compared to model spectra. As the synthetic spectrum is not use to retrieved physical properties of the stellar population, we have adopted a simple stellar library in order to better control the parameters of the fit.

After subtracting the stellar component, we measured the flux of emission lines using the SPLOT package. When the [O III] λ4959 emission line was not detected, the flux was assumed to be 0.33 times the [O III]λ5007 (the ratio of the transition probability).

3.2. A reliable estimate of the extinction

We have measured extinction by two methods in sample A: the Balmer decrement and IR/Hβ energy balance (Liang et al. 2004a). Comparing the two values, we can check the reliability

of our methodology and avoid systematic effects on abundances due to a bias in the extinction evaluation.

For 37 objects of sample A, the Hγ line was detected and we could derive extinction in the gas phase directly from the spectra, using the observed Hγ/Hβ ratio. Assuming a case B recombination with a density of 100 cm^{-3} and an electronic temperature of 10 000 K, the predicted ratio is 0.466 for $I(\mathrm{H}\gamma)/I(\mathrm{H}\beta)$ (Osterbrock 1989). Using the following relation:

$$\left(\frac{I_{\mathrm{H}\gamma}}{I_{\mathrm{H}\beta}}\right)_{\mathrm{obs}} = \left(\frac{I_{\mathrm{H}\gamma 0}}{I_{\mathrm{H}_\beta 0}}\right)_{\mathrm{intr}} 10^{-c(f(\mathrm{H}\gamma)-f(\mathrm{H}\beta))}, \quad (1)$$

we have determined the dust extinction c. The extinction parameter A_V is calculated following Seaton (1979): $A_V = E(B-V)R = (c\,R)/1.47$ where $R = 3.1$. The median extinction of the sample is $A_V = 1.53$.

Because of large uncertainties related to the measurement of the Hγ line, we needed to verify the quality of our derived extinction. Another method to evaluate A_V is from the infrared and optical SFR. Indeed, when dust extinction is taken into account, the SFR_{H_α} is in good agreement with SFR_{IR} (Flores et al. 2004). The ratio of the uncorrected extinction $SFR_{\mathrm{H}\alpha}$ and SFR_{IR} allows us to estimate the amount of extinction. The two SFR have been computed assuming the Kennicutt (1998) calibrations and both use the same Salpeter initial mass function (IMF) (Salpeter 1955). The L_{IR} is estimated from the Chary & Elbaz (2001) relation and 24 μm observations (Le Floc'h et al. 2005). The $L_{\mathrm{H}\alpha}$ has been estimated from the flux of Hβ and assuming $\mathrm{H}_\alpha/\mathrm{H}\beta = 2.87$ (Osterbrock 1989). The Hβ flux was corrected by an aperture factor derived from photometric magnitudes at I_{AB} and V_{AB} and spectral magnitudes. Finally, the ratio was corrected using the average interstellar extinction law:

$$A_V(\mathrm{IR}) = \frac{3.1}{1.66} \log \frac{SFR_{\mathrm{IR}}}{SFR_{\mathrm{H}_\alpha \mathrm{nc}}}. \quad (2)$$

The median extinction in the sample for IR/Hβ estimation is $A_V = 1.71$. In the case of objects without IR detection, we used the detection limit of 0.08 mJy of the MIPS catalogue to find an upper limit for L_{IR} and so an upper extinction limit $A_V(\mathrm{IR}_{\mathrm{lim}})$.

In Fig. 4 we compare the extinction given by the two methods. We plot in the same figure the objects from sample A+B with A_V(Balmer) and A_V(IR) measurements. The same methodology was used to determinate A_V(Balmer) and A_V(IR) in Sample B, see Liang et al. (2004a) for a complete description of the method. Most galaxies fall within the ±0.64 rms 1-σ dispersion. This result is consistent with Flores et al. (2004) and Liang et al. (2004a). We notice that the median extinction of the sample B is higher than sample A: $A_V(\mathrm{Balmer}) = 1.82$ and $A_V(\mathrm{IR}) = 2.18$. This difference between the two samples can be due to the selection of the sample B: galaxies are more luminous than in sample A and detected in near IR.

Some discrepancies between the two measurements of extinction are due to geometrical properties, as in J033212.39–274353.6, J033232.13–275105.5 and CFRS 03.0932 which show A_V(IR) greater than A_V(Balmer). Indeed, these 3 objects are edge-on galaxies. In such cases, a large fraction of the disk is hidden by the dust in the disk plane. The detected optical Balmer lines trace the star formation of a few optically thin HII regions lying on the periphery of the galaxy in the line of sight of the observer. The consequence is an underestimated extinction value. The infrared radiation is less affected by dust so it comes from deeper regions of the galaxy. Thus, we expect to have higher extinction values when estimated with the IR flux.

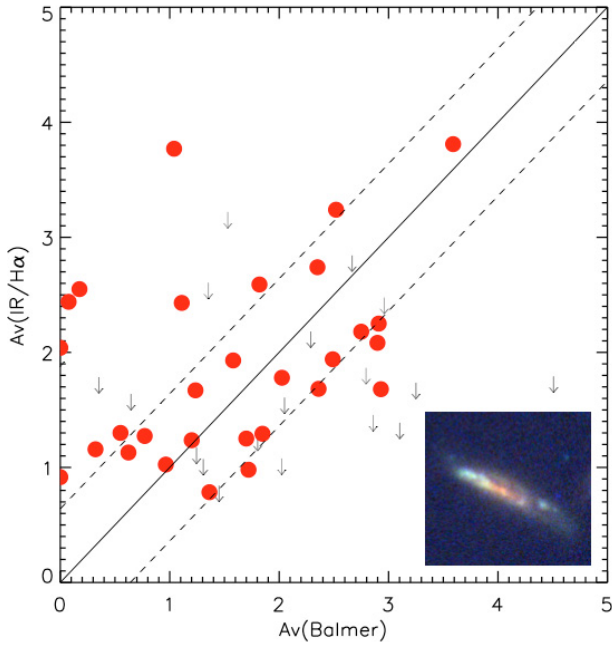

Fig. 4. Relation between the extinction A_V values derived from the Balmer decrement and by SFR_{IR} and $SFR_{\mathrm{H}_\alpha \mathrm{nc}}$ ratio. We plot the 37 galaxies from Sample A having reliable Hγ detection and the 13 galaxies from Sample B with A_V(Balmer) and A_V(IR) measurements. The objects with infrared detection are plotted with filled red circles. The arrows are the 21 objects the Sample A with only A_V(IR) upper limit estimations. The two dashed lines refer to the results with ±0.64 rms. The lower right image in the graph is the combined ACS/HST image in B, V and I band of the edge-on galaxy J033212.39–274353.6.

For non-edge-on galaxies, we have assumed that the difference between the two measurements is statistical and not intrinsic: i.e. the two extinctions are statistically equal. Hereafter, we assume A_V as the mean value between A_V(IR) and A_V(Balmer) for the objects with IR detection and the mean between $A_V(\mathrm{IR}_{\mathrm{lim}})$ and A_V(Balmer) for galaxies with an IR upper limit. For objects without Hγ detection we have used A_V(IR) or $A_V(\mathrm{IR}_{\mathrm{lim}})$ when L_{IR} is not available. For edge-on galaxies, the difference between the two extinction estimates is physical, as explained above. Since our aim is to correct the optical spectra, we have used A_V(Balmer) for these galaxies. The comparison between the two extinction estimates allows us to minimize systematic errors. In fact, A_V(IR) tends to give higher extinction values because the mid-IR light is less affected by dust. On the other hand, the Balmer decrement may underestimate the extinction because it follows only the massive star population and regions without dust-obscured star formation. Adopting the mean values between the two methods allows us to reduce the systematic errors of each one.

3.3. Searching for possible AGN contamination

Before studying metallicities in galaxies we have to identify the objects whose lines are affected by contamination from an AGN. This identification is essential because the AGN processes affect the [O III] emission lines and thus also any metallicity estimate based in this line. First, we eliminated from Sample A two galaxies harboring AGN spectral features, like broad Mg II and Balmer lines: J033208.66–274734.4 and J033230.22–274504.6. These two galaxies are very compact and are both X-ray

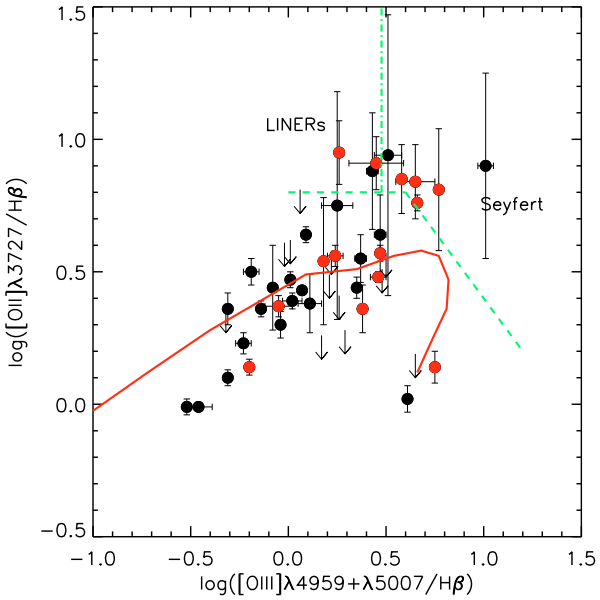

Fig. 5. Diagnostic diagram for the Sample A. Galaxies with only $A_V(\mathrm{IR_{lim}})$ are plotted with down arrows. The objects with $\log([\mathrm{Ne\,III}]\lambda3868/[\mathrm{O\,II}]\lambda3727) > -1.3$ are plotted with red dots. The solid line shows the theoretical sequence from McCall et al. (1985) for extra-galactic HII regions. The dashed line shows the photo-ionization limit for a stellar temperature of 60 000 K and empirically delimits the Seyfert 2 and LINER from the H II regions. The dot-dashed line shows the demarcation between Seyfert 2 and LINERs from Osterbrock (1989).

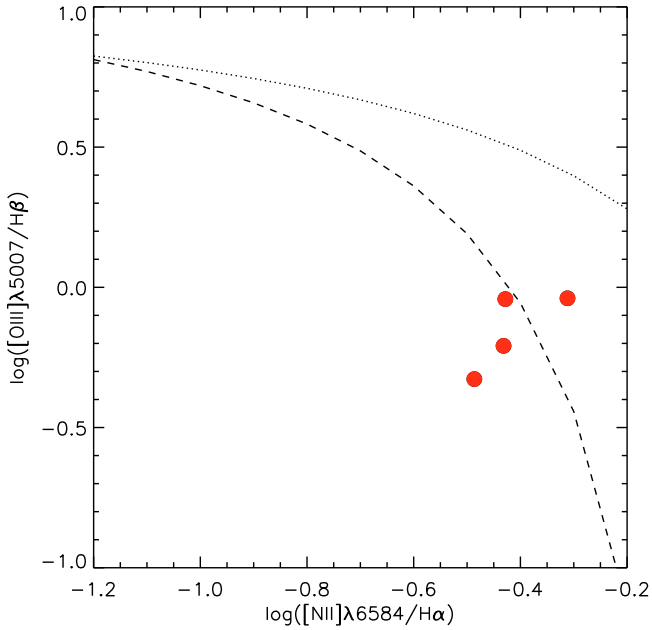

Fig. 6. Diagnostic diagram for Sample A. The doted line shows the limit of the region occupied by star-forming galaxies from Kewley et al. (2001). The dashed line represents the empirical demarcation separating star-formation galaxies from AGN from Kauffmann et al. (2003).

detected. Broad Balmer lines suggest that these galaxies are Seyfert 1 galaxies.

Then, the diagnostic diagram $\log([\mathrm{O\,II}]\,\lambda3727/\mathrm{H}_\beta)$ vs. $\log([\mathrm{O\,III}]\ \lambda\lambda4959,\ 5007/\mathrm{H}_\beta)$ was used to distinguish the H II region-like objects from LINERs and Seyfert galaxies, see Fig. 5. We have found 10 objects in the LINER and Seyfert 2 region of the excitation diagram: J033214.48–274320.1, J033219.32–274514.0, J033222.13–274344.5, J033223.06–274226.3, J033224.60–274428.1, J033229.32–275155.4, J033236.72–274406.4, J033240.04–274418.6, J033243.96–274503.5, J033245.51–275031.0. From these objects we discard 5 galaxies which fall out of the H II region, even if we account for error bars: J033219.32–274514.0, J033222.13–274344.5, J033240.04–274418.6, J033243.96–274503.5, J033245.51–275031.0. The other 5 galaxies are very close to the limit of star-forming galaxies to classify them definitely as AGN. We have chosen to keep them and we have used a different symbol for these objects in the figures.

We search for evidence of shock processes in our galaxy sample by the presence of the emission line [Ne III]$\lambda3868$. Five galaxies present $\log([\mathrm{Ne\,III}]\lambda3868/[\mathrm{O\,II}]\lambda3727) > -1.3$ and fall in the Seyfert 2 area. One of them, J033236.72–274406.4 has IR and X-ray detected.

For 4 objects, H_α and [N II] measurements are available and we have checked the $\log([\mathrm{N\,II}]\lambda\ 6584/\mathrm{H}_\alpha)$ vs. $\log([\mathrm{O\,III}]\ \lambda\lambda4959, 5007/\mathrm{H}_\beta)$ diagnostic diagram, see Fig. 6: all of them fall in the H II region delimited by Kewley & Dopita (2002).

3.4. Estimating the metallicity of the ionized gas

We have evaluated the metal abundance in the warm ionized gas. Such an estimate reflects the current metallicity of the gas from which the next generation of stars will form. Accurate metallicity measurements in the gas phase require the determination of the electron temperature T_e, usually given by the ratio of auroral to nebular line flux, such as $[\mathrm{O\,III}]\lambda\lambda4959,\ 5007/[\mathrm{O\,III}]\lambda4363$. Unfortunately, in metal-rich environments the $[\mathrm{O\,III}]\lambda4363$ line is too weak to be detected. Furthermore, even at low metallicities this auroral line is hardly detectable in low S/N spectra from high-z galaxies.

To overcome this difficulty, several estimators are used in literature based on strong emission lines. We have used the R_{23} parameter defined by Pagel et al. (1979) as $R_{23} = ([\mathrm{O\,II}]\lambda3727 + [\mathrm{O\,III}]\lambda\lambda4959,\ 5007)/\mathrm{H}\beta$. There is a large number of theoretical and empirical calibrations linking R_{23} to oxygen abundance (Pilyugin 2001; Kewley & Dopita 2002; Tremonti et al. 2004; Pilyugin & Thuan 2005; Liang et al. 2007). Abundances determined by different indicators give substantial biases and discrepancies. For example, the difference between calibrations based on electronic temperature and on photo-ionization model can reach 0.5 dex (Liang et al. 2007; Rupke et al. 2008; Kewley & Ellison 2008). As the aim of this work is to compare metallicities at different redshifts, we have adopted the calibration from Tremonti et al. (2004) to avoid a bias related to calibration:

$$12 + \log(\mathrm{O/H}) = 9.185 - 0.313x - 0.264x^2 - 0.321x^3, \qquad (3)$$

where $x = \log R_{23}$. Indeed, we want to compare sample A + B with the SDSS sample from which the Tremonti calibration is based.

The R_{23} calibration presents some limitations in abundance determination, it is double valued with $12 + \log(\mathrm{O/H})$. At low metallicity R_{23} scales with metal abundance. But from $12 + \log(\mathrm{O/H}) = 8.3$, gas cooling occurs through metallic lines and R_{23} decreases. The calibration from Tremonti et al. (2004) is valid only for the upper branch of the R_{23} vs. $12 + \log \mathrm{O/H}$ relation. We have assumed that our sample of intermediate-mass galaxies lies in the upper branch. In fact, galaxies in the extreme end of the lower branch are extremely rare and are associated

with dwarf galaxies. For moderate metallicities, near the turning point of the relation, the uncertainties in selecting the appropriate branch is smaller than the uncertainties from sky and extinction. We test this hypothesis with the [N II]/[O II] indicator. There are only 4 galaxies in our sample with [N II] measurements: all have $\log f([\mathrm{N\,II}])/f([\mathrm{O\,II}]) > -1$ and therefore belong to the upper-branch (Kewley & Dopita 2002). We think that, with a large level of confidence, all the objects lie in the upper branch of the R_{23} vs. 12 + log(O/H). Nine objects have $\log R_{23} > 1$ where the Tremonti et al. (2004) calibration is not defined. In such cases we adopted the limit given where $\log R_{23} = 1$.

For the 5 lowest redshift galaxies (type E3 in Table 2), the [O II] emission line falls out the wavelength range. We have used in this case the R_3 parameter defined by $R_3 = 1.35\times([\mathrm{O\,III}]\lambda5007/\mathrm{H}\beta)$ (Edmunds & Pagel 1984). The oxygen abundance was estimated with the calibration proposed by Vacca & Conti (1992):

$$12 + \log(\mathrm{O/H}) = -0.60 \times \log R_3 - 3.24. \quad (4)$$

We have not found any evidence of a systematic bias between the R_{23} and the R_3 calibrations. Metal abundance and the associated error are shown in Table 8.

3.5. Error budget

The uncertainties in the data were assumed to be Poisson distributed. The error budget of emission line flux includes contributions from the sky and the object. We have propagated this error on the Hγ/Hβ line ratio to estimate the error on A_V(Balmer). For A_V(IR) the error has been estimated taking into account the error on the IR luminosity and the Poisson noise of the Hβ line. As the error on A_V(Balmer) is dominated by the error on the H_γ line, we can assume that the errors on A_V(Balmer) and A_V(IR) are not correlated. Thus, the error of the final extinction depends on the error of the two extinction estimates. The errors of line ratios and metallicity have been calculated by Monte-Carlo simulation taking into account the error on extinction and the sky error on line flux.

4. Stellar mass – metallicity relation and its evolution

4.1. The stellar mass – metallicity relation at $z \sim 0.7$

We compared the metal abundance of our sample of 88 distant galaxies with those of local starbursts from SDSS (Tremonti et al. 2004). Stellar masses were estimated using absolute K band magnitude with M_{stellar}/L_K expected by observed rest frame $B - V$ color (Bell et al. 2003) and converted to a Salpeter (1955) IMF. The convertion between Kroupa (2001) and Salpeter (1955) is described in Bell et al. (2003). We found that distant galaxies are metal deficient compared to local starbursts, as shown in Fig. 7. Given the small range in stellar mass covered by our sample, it was not possible to constrain the evolution of the shape of the M-Z relation at $z \sim 0.7$. Thereafter, we assumed that the slope of the M-Z relation remained unchanged compared to the local relation. At $z \sim 0.7$ the local relation found by Tremonti et al. (2004) is shifted to lower metallicity by $\Delta[12 + \log(\mathrm{O/H})] = 0.31$ dex $\pm$ 0.03. For each galaxy we calculated the difference between its metallicity and the metallicity given by the Tremonti et al. (2004) relation for its stellar mass. The offset of the $z \sim 0.7$ relation is the median of this difference. Only galaxies with a stellar mass over the limit of completeness

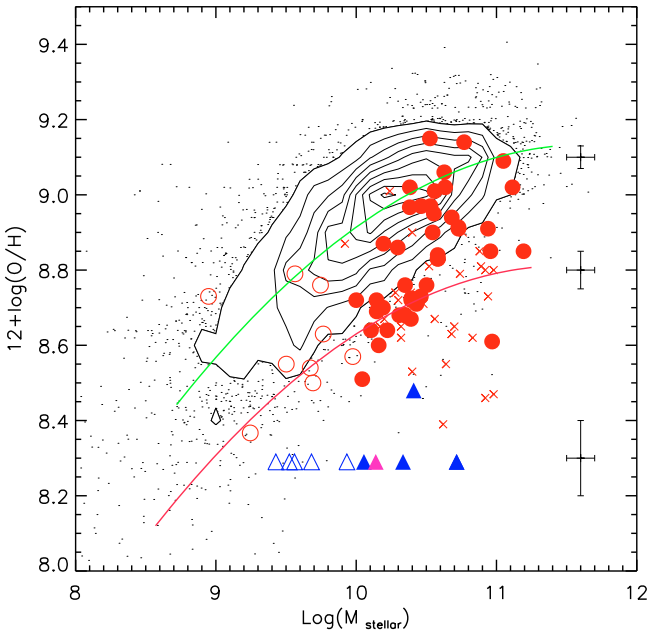

Fig. 7. Stellar mass-metallicity relation for the SDSS galaxies in contours and dots ($z = 0$, Tremonti et al. 2004, Bell et al. 2003, see text) and the 88 intermediate-z galaxies: sample A's in red circles and sample B in red crosses. Galaxies with masses lower the completeness limit $\log M_{\mathrm{stellar}} < 10$ are plotted with open symbols. The objects in sample A with $\log R_{23} > 1$ are plotted as small pink triangles and those detected as possible AGN are plotted as blue triangles. The typical error bars for bin 1, bin 2 and bin 3 are plotted on the right. The red line indicates the median of the intermediate-z relation.The green line represents the local relation fit found by Tremonti et al. (2004). The shift between the local relation and our data sample is $\Delta[12 + \log(\mathrm{O/H})] = -0.31$ dex $\pm$ 0.03.

were used. The standard error was estimated using a bootstrap method.

The shift is assumed to be only due to a metallicity evolution. Indeed, Liang et al. (2006) argue that the evolution in the M-Z relation is due to a diminution of the metal content in galaxies rather than an increase of their stellar mass. In fact, the amount of star formation necessary to increase the stellar mass by ten times would imply that almost all the light in distant galaxies is associated with a very young stellar population. However, the spectra of these galaxies show a mixture of young, intermediate and old stellar populations.

There is a large dispersion of the data around the median relation at $z \sim 0.7$, about $\pm$0.45 dex. To verify if this dispersion is intrinsic to the objects or due to the error on our data, we divided our sample into three bins. Bin 2 (3) includes the 25% of object which are the most over (under) metal abundant compared to the median. The rest of the objects constitutes bin 1. We calculated the median error of the metallicity in each bin and found: 0.05, 0.03 and 0.1 (bin 1, bin 2 and bin 3). We have plotted the mean error of each bin in Fig. 7. There is an evolution of the error of the metallicity through the 3 bins, which is well explained by the shape of the $12 + \log(\mathrm{O/H})$ vs. R_{23} calibration. Indeed, the metallicity varies rapidly with R_{23} in the metallicity range near the turn over of the function, at low metallicities. Nevertheless, the dispersion of the data in the M-Z relation is much larger that the error on metallicity. The dispersion is then intrinsic to the objects. We discuss the origin of this dispersion in Sect. 6.4.

We have searched for systematic effects due to morphological and environment properties. First we isolated the sub-sample of galaxies standing in the CDFS structures. Metal abundance

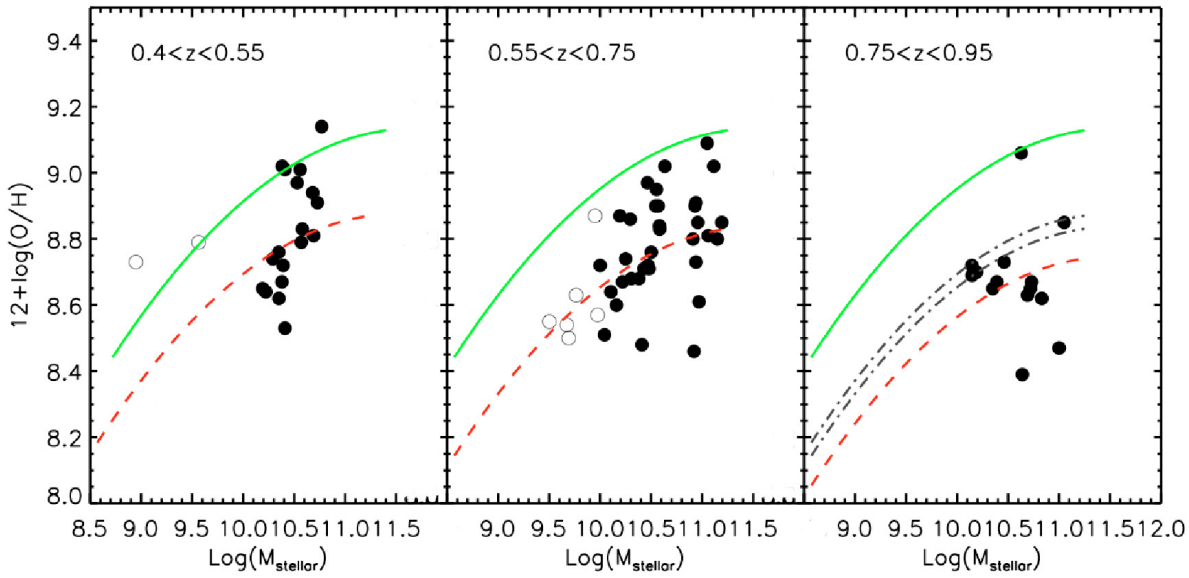

Fig. 8. Evolution of the M-Z relation inside the Sample A + B. *Left Panel*: the 17 galaxies from the $0.4 \leq z < 0.55$ bin. *Middle Panel*: the 38 galaxies from the $0.55 \leq z < 0.75$ bin. *Right Panel*: the 15 galaxies from the $0.75 \leq z \leq 0.95$ bin. The galaxies with masses under the completeness limit are plotted with open circles. Objects with $\log(R23) > 1$ and AGN are not plotted. The median of each bin is marked in dashed red line, see Table 3 for the $\Delta[12 + \log(\mathrm{O/H})]$. The local relation from Tremonti et al. (2004) is marked with a green line. Only galaxies with over the completeness limit $\log M_{\mathrm{stellar}} < 10$ have been taken to calculate the median shift. The two black lines in *the right panel* are the median of the two previous bin.

may be higher in these galaxies because of higher merger rates and then rapid galaxy evolution. Nevertheless we have not found any evidence of bias. This is probably due to an effect of data selection. The working sample majority includes starburst galaxies with intermediate mass. The evolved galaxies in structures are expected to be massive galaxies with poor star-formation.

We have also tested the effects of morphology on the locus of galaxies in the M-Z relation. We selected spiral galaxies in sample A + B (Zheng et al. 2005) and plotted them in the M-Z plot, but no effect was found.

Finally, we focused particularly on the study of LIRGs. Rupke et al. (2008) found that LIRGs and ULIRGs are metal under-abundant by a factor of two compared to emission-line galaxies in the local Universe. We have looked for evidence in the sub-sample of 20 LIRGs representing 20% of the sample A + B. We compared the LIRG metallicity with the starburst galaxies at $z \sim 0.7$ and we did not find any shift. The small metal overabundance found by Liang et al. (2006) was due to a selection effect: LIRGs in sample B are more massive and have higher redshifts than in sample A. Nevertheless, we noticed that the $z \sim 0.7$ LIRGs fall in the same locus as the local LIRGs in the M-Z relation. We will discuss these results in the Sect. 6.

4.2. Evolution to high redshift of the stellar mass – metallicity relation

One of the aims of our work is to robustly establish the evolution of the M-Z relation. We first searched for a redshift evolution of the metal content in galaxies inside the sample of intermediate redshift galaxies. As sample A + B covers a large range in redshift, from $z = 0.4$ to $z = 0.95$, we have split it into 3 redshift bins: $0.4 < z < 0.55$, $0.55 < z < 0.75$ and $0.75 < z < 0.95$. In each redshift bin, we measured the median shift of the local relation toward lower metallicity. The error of the median offset was calculated by a bootstrap method. Figure 8 shows the evolution of the M-Z relation along the 3 redshift bins. The median offsets from the local relation in the 3 bins are given in Table 3. We find

Table 3. Offset between local relation and the 3 redshift bin.

Redshift bin	$\Delta[12 + \log(\mathrm{O/H})]$	error$\Delta[12 + \log(\mathrm{O/H})]$
$0.40 \leq z < 0.55$	–0.26	0.08
$0.55 \leq z < 0.75$	–0.30	0.04
$0.75 \leq z \leq 0.95$	–0.39	0.09

an evolution of the M-Z relation from $z \sim 0.45$ to $z \sim 0.85$ of $\Delta[12 + \log(\mathrm{O/H})] = -0.13$ dex.

We then searched for an evolution of the oxygen abundance at higher redshifts. It is important that the comparison between different samples needs consistent measurements of oxygen abundance and stellar mass. In fact, particular care has to be taken when comparing metallicities from different metal estimators, especially when the aim is to evaluate the offset between samples due to an evolution in metallicity. The systematic error due to the use of different calibrations can range up to 0.5 dex and thus can be higher than the metal evolution, cf. Rupke et al. (2008). We describe below the high-z samples from the literature that have been used for this comparison.

- Liu et al. (2008) published the mass-metallicity relation for 20 galaxies from the Deep 2 Galaxy Redshift Survey at $1.0 < z < 1.5$. We only considered the 7 galaxy spectra having individual oxygen mesurements. As only [O III], Hβ, [N II] and H$_\alpha$ emission line measurements were available from the NIRSPEC/Keck observations, the $N2$ parameter was used with the Pettini & Pagel (2004) calibrator to estimate metallicity. The stellar masses were calculated from K-band photometry and the procedure proposed by Bundy et al. (2005).
- At higher redshift, $z \sim 2$, Shapley et al. (2004) observed 7 star-forming galaxies. The oxygen abundance was also estimated using the $N2$ parameter and the Pettini & Pagel (2004) calibrator. The stellar masses were calculated by fitting the spectral energy distribution to multi-band photometry.

– At the same redshift, $\langle z \rangle = 2.26$, Erb et al. (2006) have measured the metal abundance of 6 composite spectra from 87 star-forming galaxies selected by ultraviolet rest-frame and binned by stellar mass. They used the same calibration for $12 + \log(O/H)$ estimation and used the same stellar mass estimates as Shapley et al. (2004).
– Maiolino et al. (2008) presented preliminary results from the AMAZE large program to constrain the M-Z relation at $z = 3$. The oxygen abundance was measured by the R_{23} parameter and following the procedure described by Nagao et al. (2006). We only selected the 5 objects above our stellar mass completeness limit and used the R_{23} measurement to estimate the metal abundance using the Tremonti et al. (2004) calibration.

Three samples use the $N2$ parameter to evaluate the oxygen abundance. Unfortunately, metallicity estimation based on $N2$ and R_{23} can give strongly discrepant results and thus cannot be directly compared. The $N2$ parameter has several disadvantages: the [N II]/H_α ratio saturates at $12 + \log(O/H) \geq 8.8$ and becomes insensitive to the metal abundance. Furthermore, it is very sensitive to the ionization parameter and the contribution of the primary and second nitrogen whose evolution is not yet well constrained. To compare the galaxy metallicities using the $N2$ parameter we decided to re-evaluate the metallicities using the Denicoló et al. (2002) calibration. This calibration is similar to the Tremonti et al. (2004) and other R_{23} based calibrations in the working range $8.4 \leq 12 + \log(O/H) \geq 8.7$ (Kewley & Ellison 2008; Tremonti et al. 2004). For the galaxies in the sample A + B having [N II] measurements, we compared the metallicity to those of several $N2$ calibrations. We confirmed that the Denicoló et al. (2002) calibration gives similar results to the abundances estimated in this work. The M-Z diagram for the local, intermediate and high redshift samples are plotted in Fig. 9.

We have measured the median offset of the local relation and the associated error in all the high-z samples. The offset $\Delta(O/H)$ for the 3 redshift bins of the intermediate galaxies and for the four high-z samples are plotted in Fig. 10 as a function of the lookback time. We found that the evolution of the mean metallicities from the local Universe to a lookback time of ~12 Gyr is linear and with a slope given by:

$$\log Z_{tb}/Z_0 = -0.046 \times t_{Gyr}. \quad (5)$$

If the Pettini & Pagel (2004) values are used for metallicity estimates of high-z samples, the evolution remains linear with a slope of −0.051. For comparison we overplot the metallicity evolution extrapolated by Savaglio et al. (2005). The empirical evolution model was constructed by shifting the local M-Z relation in $\log M_{stellar}$ contrary to current work where the shift has been evaluated in terms of metallicity, for the reasons explained above. Their empirical model is concordant with a closed box model with an exponential star formation efficiency. We discuss in Sects. 5 and 6 the discrepancy between our observations and those of Savaglio et al. (2005), as well as the consequences for our understanding of the evolution of the M-Z relation.

5. Possible systematic uncertainties

In this section we discuss the possible systematic errors that can affect our determination of the evolution of the M-Z relation.

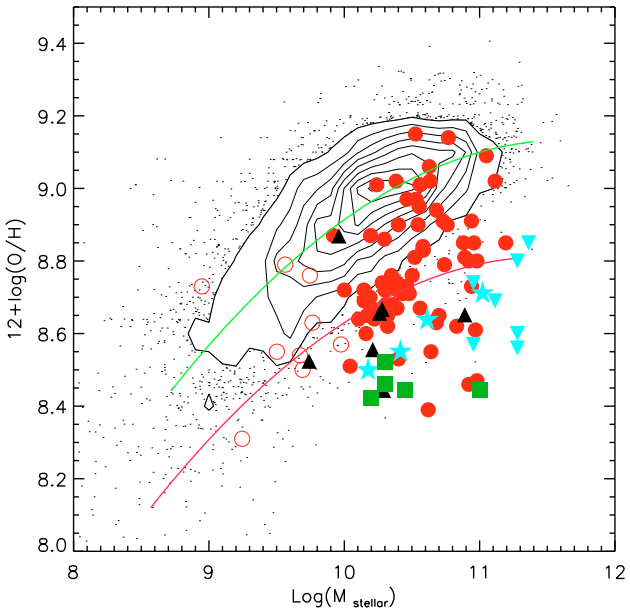

Fig. 9. Stellar mass-metallicity relation for the SDSS galaxies in contours and dots ($z = 0$, Tremonti et al. 2004; Bell et al. 2003) and the 58 intermediate-z galaxies above the completeness mass limit in red filled circle. Galaxies below the completeness mass limit are plotted with red open circles. The local relation is plotted in green (Tremonti et al. 2004) and the median of the intermediate-z relation is in red. The 7 individual galaxies at $z > 1$ of Liu et al. (2008) are plotted as black triangles. The two $z > 2$ samples are plotted in blue: inverted blue triangles indicate the 7 star-forming galaxies of Shapley et al. (2004); blue stars indicate the 5 stellar mass bin of Erb et al. (2006). The $z > 3$ sample of Maiolino et al. (2008) is plotted in green squares.

5.1. Metallicity calibrators

As we have emphasized in Sect. 3, the determination of metallicity using different calibrations may give very discrepant results. However, Kewley & Ellison (2008) have shown that the relative metallicities between galaxies can be reliably estimated within ~0.15 dex when using the same strong line calibration. In this work we have taken special care to compare our sample to the local galaxies using the same metallicity calibration and methodology. Liu et al. (2008) compared the M-Z relation at $z \sim 1$ to the local relation using $N2$ for both redshifts. They have found that $z \sim 1$ galaxies have metal abundances 0.22 dex lower than in the present Universe. This is comparable to our results.

The comparison between the metallicity at $z \sim 0.65$ and higher redshift samples is less robust: low S/N spectra and different metal indicators have been used. In fact, high-z samples usually use the $N2$ indicator. Several authors have tried to build conversions between metallicity calibrations, e.g. Kewley & Ellison (2008). However, these conversions have been derived from local samples and may be not valid at higher redshift. Liu et al. (2008) have suggested that at $z \sim 1$ the metallicities of galaxies are overestimated by ~0.16 dex due to different physical conditions in HII regions at higher redshift: violent star-formation, shocks, higher ionization parameters. No evidence of such different conditions of HII regions have been found in our sample, according to the diagnostic diagrams.

5.2. Aperture effect

The effect of aperture when comparing intermediate redshift data to the SDSS sample has been widely studied by several authors

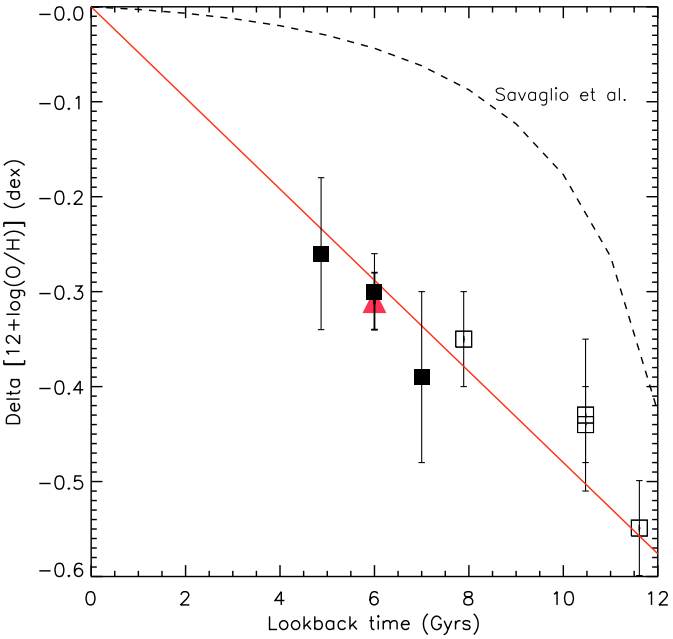

Fig. 10. The metallicity shift from the local relation of the 4 high-z samples as a function of the lookback time is plotted as black open squares. The metallicity shift for the 3 redshift bins of the IMAGES sample are in black squares and the 5 high-z data points verifying $\Delta[12 + \log(\mathrm{O/H})] = 0$ at $z = 0$. The evolution found by Savaglio et al. (2005) in the frame of a closed box model is indicated with a dashed line for $\log M_{\mathrm{stellar}} = 10.45$ galaxies.

(Savaglio et al. 2005; Liang et al. 2004a; Kobulnicky & Kewley 2004; Kewley & Ellison 2008). The SDSS observed only the center part of galaxies with a 3″ aperture fiber. The metallicities estimated are expected to be higher than the average metallicity of the galaxies because of the metallicity gradient with the distance from the center. (Vila-Costas & Edmunds 1992; Zaritsky et al. 1994; Garnett et al. 1997; Rolleston et al. 2000). Kewley & Ellison (2008) have shown that the effects is relevant for massive galaxies $M_{\mathrm{stellar}} > 10^{10}\ M_{\odot}$. However, the bias due to aperture effect in the SDSS is not larger than $Z \sim 0.1$ dex (Kewley et al. 2005) and thus has a minor impact on the estimation of the evolution of the M-Z relation.

5.3. Extinction

The effect of extinction on the estimation of metallicity is one of the main systematic errors affecting the M-Z relation. For example, an underestimation of 1.5 mag in extinction leads to an overestimation of ∼0.15 dex in oxygen abundance. Several works have assumed an average extinction to correct spectra of galaxy delimiting a large range in stellar mass. However, there is a correlation between mass and extinction (Liang et al. 2007): massive galaxies have higher extinction. Assuming a median extinction leads to an overestimation of the metallicity in massive galaxies and an underestimation in low mass system. At $z \sim 0.6$, LIRGs which have a high content of dust and gas represent 15% of the intermediate mass galaxy population. Extinction is expected to have a large impact on any abundance estimate at this redshift.

The effect of extinction may be one of the reasons for the difference between our observations and those of Savaglio et al. (2005). They have observed that the average metallicity of massive galaxies has not evolved from $z \sim 0.6$ to the present day and thus have claimed this as evidence for downsizing in metallicity. However, the majority of massive galaxies in the Savaglio et al. (2005) sample come from measurements of Lilly et al. (2003) which are from spectra with low S/N and spectral resolution. Moreover, they have applied an average $A_V = 1$ to correct emission lines. This extinction value is underestimated by about ∼1 mag for at least one third of the Lilly et al. (2003) sample, which corresponds to LIRGs. Liang et al. (2006) have estimated that the underestimation of the extinction in the Lilly et al. (2003) sample leads to an overestimation of ∼0.3 dex on metallicity, which can explain the discrepancy with our sample. The galaxies in the GDDS sample in Savaglio et al. (2005) have low luminosities and also can be affected by the low S/N of the spectra which does not allow one to retrieve proper extinction from Balmer lines for individual galaxies. These effects are amplified for evolved massive galaxies, especially those experiencing successive bursts and containing a substantial fraction of A and F stars. Unfortunately these stars are predominant in intermediate mass galaxies, and thus contaminate extinction measurement by their large Balmer absorption. Furthermore, the average extinction used by Savaglio et al. (2005) may be underestimated because the combining spectra used to measure Hγ and Hβ lines is dominated by low extinction systems.

5.4. Stellar mass

A bias in the estimation of stellar mass at high redshift must be considered. In this work, stellar masses have been estimated from the M_{stellar}/L_K ratio using the method of Bell et al. (2003). This method uses the tight correlation between rest frame optical color and M_{stellar}/L_K ratios. The amount of light due to red giant stars is corrected in the M_{stellar}/L_K using the $g - r$ colors. At higher redshift, the influence of TP-AGB stars in the derivation of the stellar masses could result in an overestimation of the stellar mass by ∼0.14 dex (Maraston et al. 2006; Pozzetti et al. 2007). However this bias has only a slight effect on the evolution of the M-Z relation. The bias in stellar mass directly translated into a systematic effect of the evolution of the M-Z relation is around –0.05 dex.

5.5. Uncertain budget

We summarize all possible sources of systematic uncertainty identified so far, in Tables 4 and 5. We expressed all uncertainties on terms of their influence in the shift of the M-Z relation from the local Universe to higher redshift. In the intermediate redshift sample we have taken particular care to diminish the bias from extinction estimates and from metallicity calibrations. Firstly, methodology has allowed us to reduce the bias due to extinction. Secondly, we used a similar methodology and the same metallicity calibrators for our sample and the local sample of Tremonti et al. (2004). The remaining systematics may come from stellar mass estimates and from the aperture effect on the SDSS data. However, as illustrated in Table 4, the systematic error from these two sources is small and thus does not change our results.

The shift of the M-Z relation from intermediate to high redshift is less secure. The sources of systematic error come from the use of different metallicity calibrations and a possible evolution of the HII properties at high-z, see Table 5. We have tried to minimize the bias from metallicity estimates selecting for the high-z sample, the metallicity calibration that better follows the one used in this work. However, even using the

Table 4. Identified systematic uncertainties that could impact on the shift of the M-Z relation between local and $z \sim 0.6$ galaxies.

Possible bias	Z	Comments
Aperture effect	0.1	See Sect. 5.2
Stellar mass	–0.05	See Sect. 5.4

Pettini & Pagel (2004) calibration instead of the Denicoló et al. (2002) calibration, we do find a linear evolution of the metal content in galaxies and with a similar slope. As the evolution of the M-Z relation is strongly constrained at $z \sim 0.6$, the bias in the high-z sample will not change the shape of the evolution function but only the slope. Even accounting for all the systematics shown in Table 5. the observations from intermediate and high redshift samples are not compatible with the evolution found by Savaglio et al. (2005).

6. Discussion

6.1. Discarding the closed-box model

We first compare our observations with a simple model of galaxy evolution: the closed-box model (Searle & Sargent 1972; Tinsley 1980). In this model galaxies are isolated systems which evolve passively transforming their gas into stars, enriching their content in metals. The amount of gas converted into stars from $z \sim 0.6$ to the present can be estimated, following the same methodology as Liang et al. (2006) and proposed by Kobulnicky & Kewley (2004). The metal abundance Z is related to the gas mass fraction by

$$Z(t) = Y \ln 1/\mu(t), \quad (6)$$

where $\mu = M_{\rm gas}/(M_{\rm gas} + M_{\rm stellar})$ is the fraction of gas. As the yield is constant the variation of metallicity depends only on the variation of the gas fraction:

$$\mathrm{d}(\log Z)/\mathrm{d}\mu = 0.434/\mu \ln \mu. \quad (7)$$

We assume that local galaxies have a gas fraction $\mu_0 = 10\%$. The metallicity of the gas phase decrease by a factor of two from $z = 0$ to $z = 0.6$. Then from Eq. (7) the gas fraction at $z = 0.6$ predicted by the closed box model is around mu = 30%. This means that the present day intermediate galaxies would have converted 20% of their present baryonic mass from gas into stars. Puech et al. (2008) studied the evolution of the Tully-Fisher relation at $z \sim 0.6$ using a representative sample of 65 emissions line intermediate galaxies. They found a significant evolution of the K-band TFR zero point, which they attribute to an average brightening by 0.66 mag. After considering several alternatives for the evolution of the stellar mass, they conclude that on average, spiral galaxies have doubled their stellar masses since $z = 0.6$. The closed box model predicts a much lower efficiency in converting gas into stars during the same elapsed time. There would be not enough gas from the closed box model to feed the stellar mass doubling. This discrepancy can be explained if ~30% of the stellar mass was formed by external gas supply, probably metal enriched (Edmunds 1990). We can definitively rule out a closed box model as a viable description of the metal content in galaxies from $z = 0.6$ to $z = 0$.

The closed box model has been taken as a first approach to explain the metal evolution of galaxies, e.g. Savaglio et al. (2005). However, we notice that the closed box model is not consistent with the two major scenarios of galaxy evolution. Indeed, to resolve the G-dwarf problem and to explain the evolution of disk, the secular scenario needs to take into account a large amount of infalling gas, e.g. primordial gas in filaments (Semelin & Combes 2005). In the hierarchical scenario the evolution of galaxies is driven by mergers and interactions, thus by gas exchange.

6.2. Comparison with previous models of galaxy chemical evolution

We compare our results with galaxy evolution simulations by de Rossi et al. (2007); Buat et al. (2008); Mouhcine et al. (2008). We have only compared the evolution of metal content in the gas phase found by the models in the same mass range as in our sample.

Within the framework of the hierarchical scenario, de Rossi et al. (2007) simulated the evolution of the M-Z relation from the present to $z = 3$. They predict very little evolution of the relation of only −0.05 dex since $z = 3$ and that massive galaxies with $M_{\rm stellar} > 3{\times}10^{10}\,M_{\odot}$ reached the local relation well before $z = 1$. Thus they predict that the spectra of massive galaxies should be mainly composed of an old metal-rich stellar population. This is in strong contradiction to our results. In our study 38% of the galaxies are above the critical mass and have strongly increased their metal content, which is consistent with the evolution of the Tully Fisher relation (Puech et al. 2008). Moreover, the results of stellar continuum fitting indicates that the predominant stellar population is composed of A and F stars, which suggest significant stellar formation 1.5 Gyr prior to our observations. The predominance of an intermediate age stellar population in galaxies at intermediate redshifts had been previously pointed out by Hammer et al. (2001).

Mouhcine et al. (2008) have simulated numerical models of galaxy evolution in the hierarchical scenario and they also predict an important downsizing effect. Metal abundances of galaxies with $M_{\rm stellar} > 10^{10}\,M_{\odot}$ have not evolved since $z \sim 1.2$. However, they found a stellar mass assembly and a metallicity dispersion consistent with our results.

Finally we compared our observations with the chemical evolution model presented by Buat et al. (2008). They investigated the star formation history of star-forming galaxies from $z = 0$ to $z = 1$ and compared it with evolution models developed for local spiral galaxies within the framework of a secular evolutionary scenario. From their model they predict the SFR and the M-Z relation evolution for intermediate mass galaxies. Their predicted evolution of metallicity is half of our observations: they predict a shift of ∼−0.2 dex at $z = 1$ (against ∼−0.4 dex in this study, see Table 3).

They also predict that at $z \sim 1$ massive galaxies have increased their metal content more rapidly than low mass galaxies, which is at odds with most current models. The Buat et al. (2008) model is based on the evolutionary history of the Milky Way, a galaxy which may not be representative of typical spirals (Hammer et al. 2007). For example, it is unlikely that the Milky Way has undergone in the past 8 Gyr strong episode of star formation such as a LIRG, which is quite common in galaxies of our sample.

At $z = 0.4$–0.9, the fraction of emission line galaxies is 60–70% (e.g. Hammer et al. 1997). Any deviations from local values in a sample of emission line galaxies is at odds with the above modelling. If we constrain Sample A to the redshift range from 0.4 to 0.7 (which limits technical problems like lines out of range), we find that 96/136 galaxies are emission line galaxies (31 with EQW(OII) < 15 and 65 with EQW(OII) > 15) and

Table 5. Identified systematic uncertainties that could impact on the shift of the M-Z relation between $z \sim 0.6$ and high-z galaxies.

Possible bias	Z	Comments
Metallicity calibration	0.3	Systhematic between $N2$ and R_{23} calibrations
Properties of H II region	–0.16	For high-z sample with $N2$ calibrations
Extinction	–0.3	R_{23} estimated sample without extinction correction
Stellar mass	–0.05	See Sect. 5.4

only 40 are absorption line galaxies. From the 65 emission lines galaxies with EQW(OII) > 15, 40 have been studied, the rest being rejected mainly for instrumental reasons (sky lines, instrument artifacts, etc.).

Thus existing modeling have difficulties in reproducing our observations, i.e. a strong evolution of the metal abundance of intermediate mass galaxies over the last 6 Gyr.

6.3. The star-formation efficiency of intermediate mass galaxies at $z \sim 0.6$

We estimate the doubling time, defined by $t_D = M_{stellar}/SFR_{IR}$, for emission line galaxies in the IMAGES sample. The SFR for galaxies without IR detection was estimated using the L_{IR} limit of detection of MIPS/Spitzer and the $SFR_{2800\ Å}$. To determine the unobscured $SFR_{2800\ Å}$, we used the UV calibration of Kennicutt (1998) and the rest-frame 2800 Å luminosity from SED fitting.

We confirm that massive galaxies convert less gas into stars than lower mass galaxies at $0.5 < z < 1$: e.g. the t_D for a massive galaxy $\log M_{stellar} = 11$ is above 3 Gyr whereas a less massive galaxy $\log M_{stellar} = 10.3$ doubles its stellar content in less than 1 Gyr. This effect is usually called "downsizing": low mass galaxies form stars at later epochs than massive galaxies. Severals authors have pointed out that downsizing is in contradiction to the hierarchical scenario. Massive galaxies form later than low mass galaxies by accretion of small dark halos, in the bottom-up scenario. However Mouri & Taniguchi (2006) and Neistein et al. (2006) have demonstrated that the downsizing of star-forming galaxies is inherent in gravitational processes of the hierarchical scenario. Low mass galaxies have very long gravitational collapse time-scales due to their small potential well. Thus they start to produce stars later than massive galaxies.

The small values of the doubling time in intermediate mass galaxies at $z \sim 0.6$ (see Fig. 12) confirm the strong evolution of these sources at this epoch. We find that the doubling time diminishes with redshift which is due to the star-formation increase with redshift. These observations are in good agreement with the results of Puech et al. (2008) who argue that galaxies have doubled their stellar mass in the last 6 Gyr.

6.4. Similarities between local LIRGs and distant starbursts & LIRGs

The IMAGES sample has enabled us to investigate several properties of distant starbursts, such as metallicity and star-formation rates, etc. These observations reveal that local LIRGs and distant starbursts/LIRGs share many properties:

– **Same locus in the M-Z relation**
Rupke et al. (2008) have shown that local LIRGs do not follow the local M-Z relation. Recall that the average SDSS galaxies populating the local M-Z plane form stars at moderate rates (less than a few solar masses per year), much lower than for starbursts and LIRGs. Local LIRGs (see

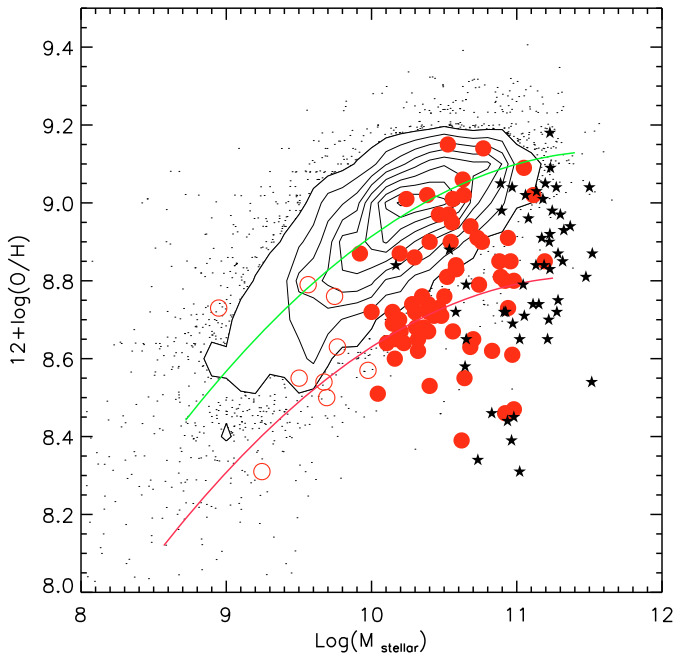

Fig. 11. M-Z relation for starburst galaxies at $z \sim 0.6$ and local LIRGs from Rupke et al. (2008). The symbols used in this plot are the same as in Fig. 9. The local LIRGs are plotted as black stars.

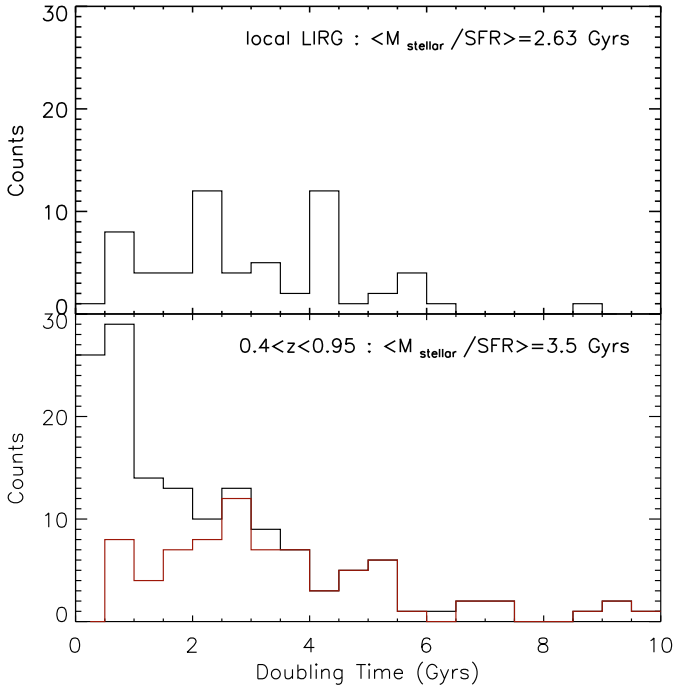

Fig. 12. Histogram of the doubling time of local LIRGs from Rupke et al. (2008) (*upper panel*) and emission line galaxies from the IMAGES sample (*botton panel*). The distribution of the IMAGES sample for galaxies delimiting the same $\log M_{stellar}$ as local LIRGS is overplotted in red.

Table 6. Basic data from galaxies in sample A. The IR luminosity of galaxies has been estimated from the mid-IR catalogue of Le Floc'h et al. (2005) and using the procedure of Chary & Elbaz (2001). The rest frame magnitude in J, K-band and the luminosity at 2800 Å have been derived by modeling galaxy SEDs using ISAAC and ACS multi-band photometry.

Name	z	RA (J2000)	Dec (J2000)	I_{AB}	L_{IR}	M_J	M_K
J033210.92–274722.8	0.417	53.04549408	−27.78966522	20.27	10.95	−21.97	−21.89
J033211.70–274507.6	0.677	53.04874039	−27.75211334	22.63	–	−19.89	−19.74
J033212.30–274513.1	0.645	53.05125809	−27.75362968	21.60	10.90	−21.89	−21.84
J033212.39–274353.6	0.422	53.05161285	−27.73155403	21.40	10.94	−21.59	−21.57
J033212.51–274454.8	0.732	53.05210876	−27.74856567	22.81	–	−19.87	−19.56
J033213.76–274616.6	0.679	53.05731201	−27.77127075	22.92	–	−19.41	−19.07
J033214.48–274320.1	0.546	53.06032181	−27.72223854	22.84	–	−19.28	−19.17
J033215.36–274506.9	0.860	53.06398392	−27.75192451	22.29	–	−21.57	−21.47
J033217.36–274307.3	0.647	53.07234955	−27.71868706	21.30	–	−21.77	−21.67
J033217.75–274547.7	0.734	53.07396698	−27.76324844	22.14	–	−21.20	−21.11
J033219.32–274514.0	0.725	53.0804863	−27.75389862	22.26	–	−21.25	−21.16
J033219.96–274449.8	0.784	53.08317947	−27.74717331	22.60	–	−20.88	−20.78
J033222.13–274344.5	0.541	53.09218979	−27.72902679	23.03	–	−19.03	−18.82
J033223.06–274226.3	0.734	53.09606552	−27.70730209	22.17	–	−21.43	−21.33
J033223.40–274316.6	0.616	53.09751511	−27.7212677	20.84	11.35	−23.00	−22.98
J033224.60–274428.1	0.538	53.10250473	−27.74114418	22.05	–	−20.47	−20.38
J033225.26–274524.0	0.666	53.10525131	−27.75665855	21.40	–	−21.63	−21.54
J033225.46–275154.6	0.672	53.10609818	−27.86517906	21.09	11.27	−22.68	−22.60
J033225.77–274459.3	0.833	53.10738373	−27.74981499	22.86	11.16	−20.94	−20.71
J033226.21–274426.3	0.495	53.10919571	−27.74064445	23.28	–	−18.59	−18.38
J033227.36–275015.9	0.769	53.11399078	−27.83775711	21.83	11.01	−21.98	−21.89
J033227.93–274353.6	0.458	53.11636734	−27.73156548	23.53	–	−17.86	−17.59
J033227.93–275235.6	0.383	53.11637878	−27.87656403	20.55	10.69	−21.59	−21.50
J033229.32–275155.4	0.510	53.12216568	−27.86540031	22.25	–	−19.42	−19.09
J033229.64–274242.6	0.667	53.12350845	−27.71182251	20.90	11.77	−22.74	−22.66
J033229.71–274507.2	0.737	53.12377548	−27.75200462	22.39	–	−20.93	−20.82
J033230.07–274534.2	0.648	53.12527084	−27.75950241	21.71	–	−21.44	−21.34
J033230.57–274518.2	0.679	53.12736893	−27.75506783	20.81	11.41	−23.00	−22.91
J033231.58–274612.7	0.654	53.13157272	−27.77020454	22.44	–	−20.35	−20.26
J033232.13–275105.5	0.682	53.13389587	−27.85154152	22.34	11.07	−21.71	−21.68
J033232.32–274343.6	0.534	53.1346817	−27.72879028	22.84	–	−19.26	−19.15
J033232.58–275053.9	0.670	53.13574982	−27.84830666	21.86	–	−21.54	−21.46
J033233.00–275030.2	0.669	53.13750839	−27.84171295	21.43	11.62	−23.18	−23.15
J033233.82–274410.0	0.666	53.1409111	−27.73611832	21.51	–	−22.61	−22.55
J033233.90–274237.9	0.619	53.14123917	−27.71053696	21.22	10.92	−21.84	−21.74
J033234.04–275009.7	0.703	53.14182281	−27.83602524	22.35	–	−20.69	−20.60
J033234.88–274440.6	0.677	53.14534378	−27.74459839	23.13	11.21	−20.65	−20.56
J033234.91–274501.9	0.665	53.14544678	−27.75053024	22.48	–	−20.42	−20.31
J033236.37–274543.3	0.435	53.15153885	−27.76201439	22.14	10.88	−21.04	−21.01
J033236.52–275006.4	0.689	53.15215683	−27.83511353	21.65	10.98	−21.78	−21.69
J033236.72–274406.4	0.666	53.1529808	−27.73512459	22.07	11.05	−22.02	−21.94
J033236.74–275206.9	0.784	53.15309906	−27.86857033	22.30	11.12	−21.39	−21.30
J033237.26–274610.3	0.736	53.15524292	−27.76953125	22.38	–	−21.15	−21.06
J033237.49–275216.1	0.423	53.15618896	−27.87112999	21.09	10.47	−20.87	−20.78
J033237.96–274652.0	0.620	53.15816498	−27.78109741	21.97	–	−20.53	−20.43
J033238.77–274732.1	0.458	53.16156006	−27.79225922	21.13	11.48	−21.32	−21.24
J033238.97–274630.2	0.420	53.16236496	−27.77506256	21.07	10.35	−21.22	−21.13
J033240.04–274418.6	0.523	53.16683197	−27.73850822	20.89	10.89	−22.02	−21.93
J033240.32–274722.8	0.619	53.16801453	−27.78967285	23.00	–	−19.62	−19.53
J033243.96–274503.5	0.533	53.1831665	−27.75096512	22.41	–	−20.16	−20.07
J033244.44–274819.0	0.416	53.18515015	−27.80527496	20.57	10.79	−22.02	−21.95
J033245.11–274724.0	0.436	53.18795013	−27.78999901	20.81	–	−22.08	−22.05
J033245.51–275031.0	0.562	53.18963242	−27.84193993	22.70	–	−19.52	−19.43
J033245.63–275133.0	0.858	53.19010544	−27.85918045	22.40	–	−21.02	−20.68
J033245.78–274812.9	0.534	53.19076157	−27.80357933	21.70	–	−21.56	−21.51
J033248.84–274531.5	0.278	53.20350266	−27.75874901	21.50	9.81	−19.56	−19.47
J033249.58–275203.1	0.415	53.20658112	−27.86752319	21.14	10.70	−21.48	−21.45
J033252.85–275207.9	0.684	53.22020721	−27.86885071	23.06	11.10	−20.64	−20.57

Fig. 11) have a deficiency in metal compared to other local galaxies and delineate the same locus in the M-Z relation as the high-z starbursts & LIRGs. Both populations show a large and similar dispersion of their metallicity at a given stellar mass. Thus local LIRGs and distant starbursts share the same metal content at a given stellar mass. Notice that in this work, we have not found differences between distant LIRGs and distant starbursts.

Table 7. The extinction A_V(Balmer), A_V(IR) and the adopted A_V. The A_V(IR) calculated with the lower limits of IR detection are upper limit. The final extinctions estimated only with the limit L_{IR} are noted with[1]. Three SFRs are given: SFR_{IR}, SFR_{Hb}, SFR_{UV}. The SFR_{Hb} is corrected for extinction and aperture. To determine the unobscured SFR_{UV}, we used the rest-frame 2800 Å luminosity from SED fitting.

Name	A_V Balmer	A_V IR	A_V	SFR_{IR} $M_\odot$ yr^{-1}	SFR_{Hb} $M_\odot$ yr^{-1}	SFR_{UV} $M_\odot$ yr^{-1}
J033210.92–274722.8	$0.77^{+0.17}_{-0.17}$	1.27 ± 0.32	$1.02^{+0.24}_{-0.25}$	15.14 ± 7.50	$11.08^{+3.82}_{-4.00}$	4.60
J033211.70–274507.6	–	<0.31	0.31[1]	<16.51	<16.58	2.04
J033212.30–274513.1	$1.85^{+0.39}_{-0.41}$	1.29 ± 0.31	$1.57^{+0.35}_{-0.36}$	13.43 ± 6.66	$18.91^{+10.22}_{-10.58}$	3.37
J033212.39–274353.6	$0.08^{+1.13}_{-0.08}$	2.44 ± 0.30	$0.08^{+1.13}_{-0.08}$	14.95 ± 4.51	$3.49^{+4.89}_{-3.49}$	1.03
J033212.51–274454.8	$1.79^{+0.40}_{-0.42}$	<0.05	$0.87^{+0.35}_{-0.37}$	<20.66	$64.07^{+34.60}_{-37.07}$	2.90
J033213.76–274616.6	–	<1.97	1.97[1]	<16.66	<16.65	1.45
J033214.48–274320.1	$1.35^{+1.15}_{-1.35}$	<2.603	$1.98^{+0.72}_{-0.84}$	<9.05	$4.19^{+6.00}_{-4.19}$	0.87
J033215.36–274506.9	$2.02^{+0.20}_{-0.20}$	<1.077	1.55 ± 0.26	<32.99	$59.06^{+22.34}_{-22.34}$	4.38
J033217.36–274307.3	–	<0.28	0.28[1]	<14.56	<14.59	5.83
J033217.75–274547.7	–	<1.70	1.70[1]	<20.87	<20.79	3.21
J033219.32–274514.0	$2.86^{+0.65}_{-0.72}$	<1.46	$2.16^{+0.47}_{-0.50}$	<20.11	$47.95^{+37.68}_{-40.91}$	2.81
J033219.96–274449.8	–	<2.17	2.17[1]	<25.17	<25.25	2.30
J033222.13–274344.5	$1.53^{+1.29}_{-1.53}$	<3.22	$2.38^{+0.78}_{-0.92}$	<8.83	$3.13^{+5.06}_{-3.13}$	0.56
J033223.06–274226.3	–	<1.91	1.91[1]	<20.84	<20.77	2.92
J033223.40–274316.6	$0.00^{+0.57}$	2.04 ± 0.30	$1.02^{+0.44}_{-0.64}$	37.95 ± 18.80	$10.79^{+7.78}_{-10.79}$	4.25
J033224.60–274428.1	$2.79^{+0.76}_{-0.85}$	<1.86	$2.33^{+0.53}_{-0.57}$	<8.70	$15.44^{+14.25}_{-15.44}$	1.65
J033225.26–274524.0	–	<1.49	1.49[1]	<15.79	<15.84	5.07
J033225.46–275154.6	–	1.71 ± 0.29	1.71 ± 0.29	32.10 ± 15.90	$31.96^{+13.75}_{-13.75}$	5.92
J033225.77–274459.3	–	0.71 ± 0.32	0.71 ± 0.32	24.86 ± 12.32	$24.92^{+12.07}_{-12.07}$	2.96
J033226.21–274426.3	$2.96^{+1.98}_{-2.77}$	<2.48	$2.72^{+1.13}_{-1.52}$	<6.92	$9.36^{+28.38}_{-9.36}$	0.51
J033227.36–275015.9	–	0.79 ± 0.31	0.79 ± 0.31	17.49 ± 8.67	17.49 ± 8.15	4.63
J033227.93–274353.6	$0.00^{+0.27}$	<2.02	$1.01^{+0.28}_{-1.06}$	<5.61	$1.62^{+0.67}_{-1.62}$	0.32
J033227.93–275235.6	$0.32^{+0.12}_{-0.12}$	1.16 ± 0.32	0.74 ± 0.22	8.46 ± 4.19	$5.05^{+1.58}_{-1.58}$	4.31
J033229.32–275155.4	$1.31^{+0.58}_{-0.64}$	<1.07	$1.19^{+0.44}_{-0.47}$	<7.52	$8.68^{+6.26}_{-6.82}$	2.18
J033229.64-274242.6	–	1.96 ± 0.32	1.96 ± 0.32	101.08 ± 50.08	$100.71^{+48.76}_{-48.76}$	7.04
J033229.71-274507.2	$2.05^{+0.63}_{-0.69}$	<1.61	$1.83^{+0.47}_{-0.50}$	<21.08	$27.74^{+21.80}_{-23.67}$	2.75
J033230.07–274534.2	$1.24^{+0.23}_{-0.23}$	<1.17	1.21 ± 0.27	<14.59	$15.27^{+6.04}_{-6.04}$	3.24
J033230.57–274518.2	$1.24^{+0.24}_{-0.25}$	1.67 ± 0.31	1.45 ± 0.28	43.69 ± 21.65	$33.30^{+13.74}_{-13.74}$	11.19
J033231.58–274612.7	$3.10^{+0.29}_{-0.31}$	<1.39	2.25 ± 0.31	<15.00	$43.41^{+20.22}_{-20.22}$	1.96
J033232.13–275105.5	$0.18^{+1.43}_{-0.18}$	2.55 ± 0.31	$0.18^{+1.43}_{-0.18}$	20.13 ± 9.98	$4.64^{+8.93}_{-4.64}$	1.40
J033232.32–274343.6	–	<1.73	1.73[1]	<8.52	<8.48	0.60
J033232.58–275053.9	–	<1.53	1.53[1]	<16.05	<16.00	3.15
J033233.00–275030.2	–	2.41 ± 0.32	2.41 ± 0.32	71.34 ± 35.35	$70.93^{+34.34}_{-34.34}$	2.38
J033233.82–274410.0	–	<2.19	2.19[1]	<15.79	<15.80	1.42
J033233.90–274237.9	$0.62^{+0.25}_{-0.26}$	1.13 ± 0.32	$0.88^{+0.28}_{-0.29}$	14.25 ± 7.06	$10.47^{+4.32}_{-4.51}$	5.71
J033234.04–275009.7	$0.65^{+0.50}_{-0.54}$	<1.64	$1.14^{+0.40}_{-0.42}$	<18.39	$9.93^{+6.34}_{-6.75}$	2.87
J033234.88–274440.6	–	2.95 ± 0.28	2.95 ± 0.28	27.90 ± 13.82	$28.00^{+11.55}_{-11.55}$	0.34
J033234.91–274501.9	–	<2.01	2.01[1]	<15.74	<15.76	1.88
J033236.37–274543.3	–	5.27 ± 0.28	5.27 ± 0.28	12.76 ± 6.32	12.69 ± 5.23	0.62
J033236.52–275006.4	$1.70^{+0.42}_{-0.45}$	1.25 ± 0.32	$1.48^{+0.37}_{-0.38}$	16.50 ± 8.17	$21.88^{+12.66}_{-13.09}$	4.78
J033236.72–274406.4	$2.90^{+1.33}_{-1.65}$	2.08 ± 0.23	$2.49^{+0.78}_{-0.94}$	19.17 ± 9.50	$31.69^{+51.27}_{-31.69}$	1.17
J033236.74–275206.9	–	1.66 ± 0.31	1.66 ± 0.31	22.68 ± 11.24	$22.57^{+10.51}_{-10.51}$	3.05

– **Similar high star formation efficiency**
Figure 12 shows the distribution of doubling times for local LIRGs (Rupke et al. 2008) and IMAGES galaxies. In order to properly compare the two samples, we used the same stellar mass range to avoid biases (e.g. shorter doubling time of low mass galaxies in the intermediate mass galaxy sample). The two distributions are very similar. The Kolmogorov-Smirnov test suggests that the probability that the two distributions arise from the same population is about 40%. We notice that stellar mass for local LIRGs has been estimated from

Table 7. continued.

Name	A_V Balmer	A_V IR	A_V	SFR_{IR} $M_\odot\,yr^{-1}$	SFR_{Hb} $M_\odot\,yr^{-1}$	SFR_{UV} $M_\odot\,yr^{-1}$
J033237.26–274610.3	$3.25^{+0.53}_{-0.57}$	<1.74	$2.49^{+0.42}_{-0.44}$	<21.02	$53.23^{+36.15}_{-38.38}$	2.44
J033237.49–275216.1	$1.36^{+0.20}_{-0.20}$	0.78 ± 0.32	1.07 ± 0.26	5.04 ± 2.50	$7.16^{+2.71}_{-2.71}$	3.19
J033237.96–274652.0	$1.80^{+0.64}_{-0.70}$	<1.28	$1.54^{+0.47}_{-0.50}$	<12.89	$17.67^{+13.89}_{-15.08}$	3.44
J033238.77–274732.1	$2.36^{+0.15}_{-0.15}$	1.68 ± 0.32	2.02 ± 0.24	51.86 ± 25.70	$78.58^{+27.08}_{-27.08}$	5.33
J033238.97–274630.2	$0.00^{+1.13}$	0.92 ± 0.31	$0.46^{+0.72}_{-0.46}$	3.83 ± 1.90	$2.18^{+3.12}_{-1.67}$	2.18
J033240.04–274418.6	–	2.21 ± 0.26	2.21 ± 0.26	13.26 ± 6.57	$13.28^{+5.02}_{-5.02}$	1.68
J033240.32–274722.8	$2.29^{+1.10}_{-1.30}$	<2.18	$2.24^{+0.68}_{-0.79}$	<12.85	$13.81^{+18.14}_{-13.81}$	1.06
J033243.96–274503.5	$4.51^{+0.93}_{-1.07}$	<1.79	$3.15^{+0.62}_{-0.69}$	<8.47	$45.28^{+52.02}_{-45.28}$	1.15
J033244.44–274819.0	$1.20^{+0.26}_{-0.27}$	1.24 ± 0.32	1.22 ± 0.29	10.62 ± 5.26	$10.41^{+4.48}_{-4.48}$	2.46
J033245.11–274724.0	$2.10^{+0.39}_{-0.41}$	<0.84	$1.15^{+0.34}_{-0.36}$	20.8	$7.16^{+3.73}_{-4.01}$	1.93
J033245.51–275031.0	$2.67^{+0.77}_{-0.87}$	<2.84	$2.75^{+0.54}_{-0.58}$	<9.80	$8.73^{+8.27}_{-8.73}$	0.78
J033245.63–275133.0	$0.35^{+0.34}_{-0.35}$	<1.79	$1.07^{+0.33}_{-0.33}$	<32.70	$13.53^{+6.80}_{-6.80}$	4.13
J033245.78–274812.9	–	<2.18	2.18[1]	<8.52	<8.54	0.72
J033248.84–274531.5	$0.96^{+0.62}_{-0.68}$	1.02 ± 0.31	$0.99^{+0.46}_{-0.49}$	1.11 ± 0.55	$1.06^{+0.81}_{-0.88}$	0.36
J033249.58–275203.1	$2.03^{+0.48}_{-0.52}$	1.78 ± 0.32	$1.90^{+0.40}_{-0.42}$	8.56 ± 4.24	$9.93^{+6.34}_{-6.74}$	1.32
J033252.85–275207.9	–	2.20 ± 0.31	2.20 ± 0.31	21.64 ± 10.72	$21.55^{+10.04}_{-10.04}$	0.64

their absolute magnitude M_K and assuming an $M/L_K = 1$. This crude assumption can lead to a slight overestimation of their stellar mass (by ∼0.1 dex) although it does not affect the overall result.

– **Similar morphologies: dominated by mergers and spirals** Severals studies in the local Universe have pointed out the link between LIRGs and merging of gas-rich spirals (Veilleux et al. 2002; Sanders & Ishida 2004; Wang et al. 2006). At higher redshifts a significant fraction of the distant galaxies have morphologies that include spiral to peculiar (Zheng et al. 2005; Neichel et al. 2008). Distant LIRGs are also associated with mergers at different stages or with large disks (Zheng et al. 2005; Flores et al. 1999).

Fundamental properties such as morphologies, star formation efficiency and mass-metallicity are similar for both local LIRGs and distant starburst/LIRGs. We may thus wonder whether local LIRGs and distant starbursts also share the same physical mechanisms explaining their properties. The only discrepancy between the two populations is their numerical abundance: while local LIRGs only represent 0.5% of the local massive galaxies, distant starbursts studied here represent approximatively 60% of distant massive galaxies (Hammer et al. 1997). We suggest that local LIRGs are the latecomers of the main population of massive starburst galaxies visible at $z \sim 0.6$.

What is the physical process explaining the properties of these two galaxy populations of actively star forming galaxies? Since star formation increases the abundance of a system, the only processes that can reduce it is gas motion (Edmunds 1990; Köppen & Edmunds 1999; Dalcanton 2007). For local LIRGs, Rupke et al. (2008) have proposed that the encounter between two gas-rich galaxies causes lower metal abundance gas from the outer regions to fall into the merger central region, providing dilution of the metal abundance. The input of gas powers the star formation and dilutes metals at the same time, explaining their location in the M-Z relationship. Independently, Hammer et al. (2005) suggested a scenario in which present spiral galaxies are built by the gradual infall of the gas being expelled during the first stages of a major merger. Both scenarios are based on supply of unprocessed gas from the outskirts of encounters during a merger event. For both cases, outflows are unlikely to be the cause of the gas dilution as they may be dominated by a neutral phase with the metal abundance of the central regions (Rupke et al. 2008, 2005).

Because distant starbursts & LIRGs are a common phenomenon in the distant Universe, a merger scenario to explain their properties may have a considerable impact on the formation of present-day spirals. This prompted Hammer et al. (2005) to propose a scenario of disk rebuilding for the majority of spirals galaxies. Recent simulations of Lotz et al. (2008) indicate that the majority of mergers can reconstruct a low mass star-forming disk. Moreover, the large dispersion in metallicity we observed at intermediate redshifts is qualitatively consistent with the diversity of galaxy-building histories within the framework of a merger scenario.

The external gas supply through merger process is in good agreement with Damped Lyman Absorber (DLA) observations. DLAs have a lower metal content compared to emission selected galaxies and have a wide dispersion in metallicity. Absorption measurements through DLAs trace outer regions of galaxies and probably extend envelopes of unprocessed gas on the outskirts of galaxies. Wolfe et al. (2003) have proposed a scenario for the formation of spiral galaxies from DLAs in which disk galaxies are surrounded by halo of neutral gas during their assembly. The simulations of Navarro (2004) and Governato et al. (2007) have reproduced many properties of local spiral galaxies by merger of gas rich encounters.

7. Conclusions

We have observed 88 intermediate mass galaxies with high quality spectra and moderate resolution to establish a robust study of the stellar mass-metallicity relation at $z \sim 0.6$. Metal abundances have been estimated following a careful analysis of each individual spectrum: evaluation of underlying absorption in Balmer lines by stellar continuum subtraction, robust extinction measurement and evaluation of AGN contamination.

Table 8. Some important emission line ratios, the oxygen abundance in the ISM and stellar mass. The uncertainties of the line ratio and metallicity are from uncertainties of extinction and emission line flux measurement. Galaxies in which extinctions have been estimated only with $A_V(IR_{\rm lim})$ are lower limits of metallicity. When $\log R_{23} > 1$ the oxygen abundance is indicated with[1]).

Name	z	$\log \frac{[\rm O\,II]}{\rm H\beta}$	$\log \frac{[\rm O\,III]}{\rm H\beta}$	$\log \frac{[\rm Ne\,III]}{[\rm O\,II]}$	$12 + \log$ O/H	$\log \frac{M}{M_\odot}$
J033210.92–274722.8	0.416	0.36 ± 0.02	−0.14 ± 0.01	–	8.94 ± 0.01	10.68
J033211.70–274507.6	0.676	0.19 ± 0.01	0.65 ± 0.01	–	>8.63	9.76
J033212.30–274513.1	0.645	0.23 ± 0.04	−0.23 ± 0.04	–	9.02 ± 0.03	10.63
J033212.39–274353.6	0.422	0.43 ± 0.52	0.07 ± 0.06	–	8.83 ± 0.35	10.58
J033212.51–274454.8	0.732	0.14 ± 0.04	0.75 ± 0.01	–0.66	8.54 ± 0.01	9.67
J033213.76–274616.6	0.679	0.57 ± 0.02	0.5 ± 0.01	–	>8.55	9.50
J033214.48–274320.1	0.546	0.94 ± 0.21	0.51 ± 0.03	–	8.29[1]	9.56
J033215.36–274506.9	0.860	0.54 ± 0.25	0.18 ± 0.01	–1.82	8.73 ± 0.19	10.46
J033217.36–274307.3	0.647	0.27 ± 0.19	0.17 ± 0.01	–	>8.90	10.54
J033217.75–274547.7	0.734	0.58 ± 0.04	0.22 ± 0.01	–	>8.68	10.31
J033219.32–274514.0	0.725	0.95 ± 0.04	0.26 ± 0.02	–1.56	8.29[1]	10.33
J033219.96–274449.8	0.784	0.62 ± 0.04	0.01 ± 0.03	–	>8.70	10.19
J033222.13–274344.5	0.541	1.05 ± 0.17	0.6 ± 0.02	–	8.29[1]	9.43
J033223.06–274226.3	0.734	0.81 ± 0.14	0.06 ± 0.12	–	>8.48	10.41
J033223.40–274316.6	0.615	0.26 ± 0.06	−0.33 ± 0.03	–	9.02 ± 0.03	11.11
J033224.60–274428.1	0.538	0.88 ± 0.1	0.43 ± 0.02	–	8.29[1]	10.05
J033225.26–274524.0	0.666	0.49 ± 0.01	0.21 ± 0.02	–1.22	>8.76	10.50
J033225.46–275154.6	0.672	0.37 ± 0.04	−0.05 ± 0.07	–1.47	8.91 ± 0.04	10.94
J033225.77–274459.3	0.832	0.02 ± 0.05	0.61 ± 0.01	–	8.72 ± 0.01	10.14
J033226.21–274426.3	0.495	–	0.65 ± 0.06	–	>8.31	9.24
J033227.36–275015.9	0.769	0.14 ± 0.01	−0.2 ± 0.02	–1.31	9.06 ± 0.01	10.63
J033227.93–274353.6	0.458	0.44 ± 0.04	0.35 ± 0.01	–	8.73 ± 0.02	8.95
J033227.93–275235.6	0.383	−0.01 ± 0.03	−0.52 ± 0.01	–	9.15 ± 0.01	10.52
J033229.32–275155.4	0.510	0.85 ± 0.07	0.58 ± 0.02	–1.23	8.29[1]	9.52
J033229.64–274242.6	0.667	0.5 ± 0.05	−0.19 ± 0.04	–	8.85 ± 0.04	10.96
J033229.71–274507.2	0.737	0.44 ± 0.09	−0.08 ± 0.02	–	8.87 ± 0.06	10.19
J033230.07–274534.2	0.648	0.54 ± 0.07	0.22 ± 0.01	–	8.71 ± 0.06	10.43
J033230.57–274518.2	0.679	0.1 ± 0.03	−0.31 ± 0.01	–	9.09 ± 0.01	11.05
J033231.58–274612.7	0.654	0.57 ± 0.04	0.47 ± 0.01	–1.03	8.57 ± 0.03	9.97
J033232.13–275105.5	0.682	0.39 ± 0.83	0.02 ± 0.04	–1.21	8.84 ± 0.59	10.58
J033232.32–274343.6	0.534	0.41 ± 0.1	0.26 ± 0.13	–	>8.79	9.56
J033232.58–275053.9	0.670	0.36 ± 0.01	−0.32 ± 0.01	–	>8.97	10.46
J033233.00–275030.2	0.669	0.28 ± 0.04	0.29 ± 0.02	–1.19	>8.85	11.19
J033233.82–274410.0	0.666	0.51 ± 0.01	0.48 ± 0.1	–	>8.61	10.97
J033233.90–274237.9	0.619	0.47 ± 0.03	0.01 ± 0.01	–	8.83 ± 0.02	10.58
J033234.04–275009.7	0.703	0.55 ± 0.05	0.37 ± 0.02	–	8.64 ± 0.03	10.10
J033234.88–274440.6	0.677	0.64 ± 0.04	0.27 ± 0.04	–	8.60 ± 0.04	10.16
J033234.91–274501.9	0.665	0.61 ± 0.01	−0.02 ± 0.05	–	>8.72	10.00
J033236.37–274543.3	0.435	–	0.13 ± 0.01	–	8.76 ± 0.01	10.35
J033236.52–275006.4	0.689	0.3 ± 0.05	−0.04 ± 0.01	–	8.95 ± 0.03	10.55
J033236.72–274406.4	0.666	0.84 ± 0.14	0.65 ± 0.1	–1.14	8.29[1]	10.71
J033236.74–275206.9	0.784	0.64 ± 0.03	0.09 ± 0.01	–	8.67 ± 0.03	10.39
J033237.26–274610.3	0.736	0.38 ± 0.07	0.11 ± 0.06	–	8.86 ± 0.06	10.29
J033237.49–275216.1	0.423	0.48 ± 0.02	0.46 ± 0.04	–1.57	8.64 ± 0.04	10.22
J033237.96–274652.0	0.619	0.63 ± 0.07	0.47 ± 0.02	–	8.51 ± 0.05	10.04
J033238.77–274732.1	0.458	–	0.06 ± 0.01	–	8.72 ± 0.01	10.39

We confirmed the shift of about ∼0.3 dex to lower abundances of the M-Z relation at $z \sim 0.6$ which was found by Liang et al. (2006). Combined with the robust selection of our sample, the relatively high number of studied galaxies in this study allows us to derive the evolution of $[12 + \log(\rm O/H)]$ over the redshift bin $0.4 < z < 0.9$. It shows that the median metal

Table 8. continued.

Name	z	$\log \frac{[\mathrm{O\,II}]}{\mathrm{H}\beta}$	$\log \frac{[\mathrm{O\,III}]}{\mathrm{H}\beta}$	$\log \frac{[\mathrm{Ne\,III}]}{[\mathrm{O\,II}]}$	$12 + \log \mathrm{O/H}$	$\log \frac{M}{M_\odot}$
J033238.97–274630.2	0.419	–	−0.34 ± 0.01	–	9.02 ± 0.01	10.38
J033240.04–274418.6	0.523	0.91 ± 0.1	0.45 ± 0.14	–1.04	8.29[1]	10.72
J033240.32–274722.8	0.619	0.75 ± 0.14	0.25 ± 0.05	–	8.50 ± 0.14	9.69
J033243.96–274503.5	0.533	0.9 ± 0.16	1.01 ± 0.02	–	8.29[1]	9.93
J033244.44–274819.0	0.416	–	−0.26 ± 0.01	–	8.91 ± 0.01	10.73
J033245.11–274724.0	0.436	−0.01 ± 0.01	−0.47 ± 0.07	–	9.14 ± 0.01	10.77
J033245.51–275031.0	0.562	0.81 ± 0.11	0.77 ± 0.01	–0.94	8.29[1]	9.68
J033245.63–275133.0	0.858	0.56 ± 0.04	0.24 ± 0.04	–1.21	8.69 ± 0.05	10.15
J033245.78–274812.9	0.534	0.21 ± 0.02	−0.1 ± 0.01	–	>9.01	10.56
J033248.84–274531.5	0.278	0.36 ± 0.08	0.38 ± 0.01	–1.18	8.76 ± 0.04	9.74
J033249.58–275203.1	0.415	0.36 ± 0.06	−0.31 ± 0.01	–	8.97 ± 0.04	10.53
J033252.85–275207.9	0.684	0.76 ± 0.03	0.66 ± 0.01	–0.89	8.29[1]	10.14

abundance of galaxies diminishes with redshift. Using similar measurements from samples at higher redshift we recover the evolution in metals in the ionised gas from $z = 0$ to $z \sim 3$: we find a linear evolution of metallicity as a function of the look-back time. This simply means that the evolution of the gas phase in massive galaxies is still active down to $z = 0.4$ unlike to the popular belief that all massive galaxies have their stellar content locked after $z = 1$.

Our results are thus in strong disagreement with those of Savaglio et al. (2005) et al. They found that the evolution of galaxies at first order can be explained by a closed box model and that galaxies with $\log M_{\mathrm{stellar}} > 10^{10}\ M_\odot$ have already reached local metallicities at $z \sim 0.6$. On the contrary, we have discarded the closed box model as a valid approximation of galaxy evolution. We suggest that this discrepancy is due to the low S/N quality of the Savaglio et al. (2005) data. We notice however that the Savaglio et al. (2005) results have been widely used to construct metal content evolution simulations, explaining why our results are not reproduced by these models. We are calling for a new generation of modelling able to account for our observations.

We have shown the need for a significant contribution of external gas supply in the metal content evolution of galaxies. From 6 Gyr ago, a significant fraction of massive galaxies have undergone a rapid growth in which 30% of their present stellar mass has been formed from an external gas supply. The addition of gas in galaxies explains the metal deficiency of star-forming galaxies at $z \sim 0.6$ at all mass scales. The origin of the gas supply is a key question. In the secular scenario, the infalling gas comes from pristine gas in the large scale filament structures. The perturbed kinematics and morphology of the intermediate redshift galaxies have lead us to favor the hierarchical scenario where the unprocessed gas could arise from large envelopes of gas lying in the halo of galaxies after merging events.

We have shown that local LIRGs and distant starbursts and LIRGs share similar properties such as star-formation efficiency, metal abundance and morphology. We suggest a unique evolution scenario for both populations, which is linked to the gas infall provided by galaxy merging and interactions. Progenitors of spiral galaxies have their disks rebuilt through an infall of the gas which has been previously expelled in the first stage of a gas-rich merger. Local LIRGs are in this case latecomers of the starburst/LIRG population predominant at $z \sim 0.6$. A better understanding of the kinematics and metallicity of galactic halos in gas-rich systems at intermediate redshift is needed to disentangle the origin of the external gas supply.

Acknowledgements. This work is supported by a Ph.D. scholarship from Fundação para a Ciencia e a Tecnologia, grants from Region Ile-de-France, the National Basic Research Program of China (973 Program) No. 2007CB815404 and the Knowledge Innovation Program of the Chinese Academy of Sciences. We thank Ana Mourão for improving the English of the text.

References

Afonso, J., Mobasher, B., Koekemoer, A., Norris, R. P., & Cram, L. 2006, AJ, 131, 1216
Arnouts, S., Vandame, B., Benoist, C., et al. 2001, A&A, 379, 740
Asari, N. V., Cid Fernandes, R., Stasińska, G., et al. 2007, MNRAS, 381, 263
Asplund, M., Grevesse, N., Sauval, A. J., Allende Prieto, C., & Kiselman, D. 2004, A&A, 417, 751
Bell, E. F., McIntosh, D. H., Katz, N., & Weinberg, M. D. 2003, ApJS, 149, 289
Bell, E. F., Papovich, C., Wolf, C., et al. 2005, ApJ, 625, 23
Bruzual, G., & Charlot, S. 2003, MNRAS, 344, 1000
Buat, V., Boissier, S., Burgarella, D., et al. 2008, A&A, 483, 107
Bundy, K., Ellis, R. S., & Conselice, C. J. 2005, ApJ, 625, 621
Cardelli, J. A., Clayton, G. C., & Mathis, J. S. 1989, ApJ, 345, 245
Chary, R., & Elbaz, D. 2001, ApJ, 556, 562
Cid Fernandes, R., Mateus, A., Sodré, L., Stasińska, G., & Gomes, J. M. 2005, MNRAS, 358, 363
Dalcanton, J. J. 2007, ApJ, 658, 941
de Rossi, M. E., Tissera, P. B., & Scannapieco, C. 2007, MNRAS, 374, 323
Denicoló, G., Terlevich, R., & Terlevich, E. 2002, MNRAS, 330, 69
Edmunds, M. G. 1990, MNRAS, 246, 678
Edmunds, M. G., & Pagel, B. E. J. 1984, MNRAS, 211, 507
Erb, D. K., Shapley, A. E., Pettini, M., et al. 2006, ApJ, 644, 813
Flores, H., Hammer, F., Thuan, T. X., et al. 1999, ApJ, 517, 148
Flores, H., Hammer, F., Elbaz, D., et al. 2004, A&A, 415, 885
Garnett, D. R., Shields, G. A., Skillman, E. D., Sagan, S. P., & Dufour, R. J. 1997, ApJ, 489, 63
Giacconi, R., Zirm, A., Wang, J., et al. 2002, ApJS, 139, 369
Giavalisco, M., Ferguson, H. C., Koekemoer, A. M., et al. 2004, ApJ, 600, L93
Governato, F., Willman, B., Mayer, L., et al. 2007, MNRAS, 374, 1479
Hammer, F., Flores, H., Lilly, S. J., et al. 1997, ApJ, 481, 49
Hammer, F., Gruel, N., Thuan, T. X., Flores, H., & Infante, L. 2001, ApJ, 550, 570
Hammer, F., Flores, H., Elbaz, D., et al. 2005, A&A, 430, 115
Hammer, F., Puech, M., Chemin, L., Flores, H., & Lehnert, M. D. 2007, ApJ, 662, 322
Jacoby, G. H., Hunter, D. A., & Christian, C. A. 1984, ApJS, 56, 257
Kauffmann, G., Heckman, T. M., Tremonti, C., et al. 2003, MNRAS, 346, 1055

Kennicutt, Jr., R. C. 1998, ARA&A, 36, 189
Kewley, L. J., & Dopita, M. A. 2002, ApJS, 142, 35
Kewley, L. J., & Ellison, S. L. 2008, [arXiv:0801.1849]
Kewley, L. J., Heisler, C. A., Dopita, M. A., & Lumsden, S. 2001, ApJS, 132, 37
Kewley, L. J., Jansen, R. A., & Geller, M. J. 2005, PASP, 117, 227
Kobulnicky, H. A., & Kewley, L. J. 2004, ApJ, 617, 240
Köppen, J., & Edmunds, M. G. 1999, MNRAS, 306, 317
Kroupa, P. 2001, MNRAS, 322, 231
Lamareille, F., Contini, T., Charlot, S., & Brinchmann, J. 2007, IAU Symp. 235, ed. F. Combes, & J. Palous, 408
Le Floc'h, E., Papovich, C., Dole, H., et al. 2005, ApJ, 632, 169
Lequeux, J., Peimbert, M., Rayo, J. F., Serrano, A., & Torres-Peimbert, S. 1979, A&A, 80, 155
Liang, Y. C., Hammer, F., Flores, H., et al. 2004a, A&A, 423, 867
Liang, Y. C., Hammer, F., Flores, H., Gruel, N., & Assémat, F. 2004b, A&A, 417, 905
Liang, Y. C., Hammer, F., & Flores, H. 2006, A&A, 447, 113
Liang, Y. C., Hammer, F., Yin, S. Y., et al. 2007, A&A, 473, 411
Lilly, S. J., Carollo, C. M., & Stockton, A. N. 2003, ApJ, 597, 730
Liu, X., Shapley, A. E., Coil, A. L., Brinchmann, J., & Ma, C.-P. 2008, ApJ, 678, 758
Lotz, J. M., Jonsson, P., Cox, T. J., & Primack, J. R. 2008, [arXiv:0805.1246]
Maier, C., Lilly, S. J., Carollo, C. M., et al. 2006, ApJ, 639, 858
Maiolino, R., Nagao, T., Grazian, A., et al. 2008, A&A, 488, 463
Maraston, C., Daddi, E., Renzini, A., et al. 2006, ApJ, 652, 85
McCall, M. L., Rybski, P. M., & Shields, G. A. 1985, ApJS, 57, 1
Mouhcine, M., Gibson, B. K., Renda, A., & Kawata, D. 2008, [arXiv:0801.2476]
Mouri, H., & Taniguchi, Y. 2006, A&A, 459, 371
Nagao, T., Maiolino, R., & Marconi, A. 2006, A&A, 459, 85
Navarro, J. F. 2004, in Penetrating Bars Through Masks of Cosmic Dust, ed. D. L. Block, I. Puerari, K. C. Freeman, R. Groess, & E. K. Block, Astrophysics and Space Science Library, 319, 655
Neichel, B., Hammer, F., Puech, M., et al. 2008, A&A, 484, 159
Neistein, E., van den Bosch, F. C., & Dekel, A. 2006, MNRAS, 372, 933
Osterbrock, D. E. 1989, Astrophysics of gaseous nebulae and active galactic nuclei, Research supported by the University of California, John Simon Guggenheim Memorial Foundation, University of Minnesota (Mill Valley CA: University Science Books), 422
Pagel, B. E. J., Edmunds, M. G., Blackwell, D. E., Chun, M. S., & Smith, G. 1979, MNRAS, 189, 95
Pettini, M., & Pagel, B. E. J. 2004, MNRAS, 348, L59
Pilyugin, L. S. 2001, A&A, 369, 594
Pilyugin, L. S., & Thuan, T. X. 2005, ApJ, 631, 231
Pozzetti, L., Cimatti, A., Zamorani, G., et al. 2003, A&A, 402, 837
Pozzetti, L., Bolzonella, M., Lamareille, F., et al. 2007, A&A, 474, 443
Puech, M., Flores, H., Hammer, F., et al. 2008, A&A, 484, 173
Ravikumar, C. D., Puech, M., Flores, H., et al. 2007, A&A, 465, 1099
Rolleston, W. R. J., Smartt, S. J., Dufton, P. L., & Ryans, R. S. I. 2000, A&A, 363, 537
Rupke, D. S., Veilleux, S., & Sanders, D. B. 2005, ApJS, 160, 115
Rupke, D. S. N., Veilleux, S., & Baker, A. J. 2008, ApJ, 674, 172
Salpeter, E. E. 1955, ApJ, 121, 161
Sanders, D., & Ishida, C. 2004, in The Neutral ISM in Starburst Galaxies, ed. S. Aalto, S. Huttemeister, & A. Pedlar, ASP Conf. Ser., 320, 230
Savaglio, S., Glazebrook, K., Le Borgne, D., et al. 2005, ApJ, 635, 260
Searle, L., & Sargent, W. L. W. 1972, ApJ, 173, 25
Seaton, M. J. 1979, MNRAS, 187, 73P
Semelin, B., & Combes, F. 2005, A&A, 441, 55
Shapley, A. E., Erb, D. K., Pettini, M., Steidel, C. C., & Adelberger, K. L. 2004, ApJ, 612, 108
Tinsley, B. M. 1980, A&A, 89, 246
Tremonti, C. A., Heckman, T. M., Kauffmann, G., et al. 2004, ApJ, 613, 898
Vacca, W. D., & Conti, P. S. 1992, ApJ, 401, 543
Veilleux, S., Kim, D.-C., & Sanders, D. B. 2002, ApJS, 143, 315
Vila-Costas, M. B., & Edmunds, M. G. 1992, MNRAS, 259, 121
Wang, J. L., Xia, X. Y., Mao, S., et al. 2006, ApJ, 649, 722
Wolfe, A. M., Gawiser, E., & Prochaska, J. X. 2003, ApJ, 593, 235
Yang, Y., Flores, H., Hammer, F., et al. 2008, A&A, 477, 789
Zaritsky, D., Kennicutt, Jr., R. C., & Huchra, J. P. 1994, ApJ, 420, 87
Zheng, X. Z., Hammer, F., Flores, H., Assémat, F., & Rawat, A. 2005, A&A, 435, 507